



Contents lists available at ScienceDirect

International Journal of Solids and Structures

journal homepage: www.elsevier.com/locate/ijsolstr

Local slamming impact of sandwich composite hulls

Z. Qin*, R.C. Batra

Department of Engineering Science and Mechanics, Virginia Polytechnic Institute and State University, Blacksburg, VA 24061-0219, USA

ARTICLE INFO

Article history:

Received 22 January 2008

Received in revised form 24 April 2008

Available online 3 May 2008

Dedicated to the memory of late Professor Liviu Librescu who sacrificed his life to save lives of students in his class during the 16 April 2007 tragedy at Virginia Tech.

Keywords:

Sandwich composite hulls
Slamming impact
Hydroelastic effect
Unsteady slamming load
Fluid–structure interaction

ABSTRACT

We develop a hydroelastic model based on a {3,2}-order sandwich composite panel theory and Wagner's water impact theory for investigating the fluid–structure interaction during the slamming process. The sandwich panel theory incorporates the transverse shear and the transverse normal deformations of the core, while the face sheets are modeled with the Kirchhoff plate theory. The structural model has been validated with the general purpose finite element code ABAQUS®. The hydrodynamic model, based on Wagner's theory, considers hull's elastic deformations. A numerical procedure to solve the nonlinear system of governing equations, from which both the fluid's and the structure's deformations can be simultaneously computed, has been developed and verified. The hydroelastic effect on hull's deformations and the unsteady slamming load have been delineated. This work advances the state of the art of analyzing hydroelastic deformations of composite hulls subjected to slamming impact.

Published by Elsevier Ltd.

1. Introduction

Bottom slamming is caused by impact between a running marine vessel and the water (see e.g., Bishop et al., 1978; Faltinsen, 1990; Mizoguchi and Tanizawa, 1996). In most cases, it is the result of a series of large pitch and heave motions that force a part of the vessel bottom to emerge out of water and subsequently reenter the water. The generated load is typically characterized by very short-duration (e.g., of a few milliseconds), acting on a small surface and high-peak pressure. The impact can cause severe local damage to the hull, material/structural failure by fatigue, injury to occupants due to high acceleration, or in a benign case, globally uncomfortable high-frequency vibrations. Due to the severity and significance of such phenomena on marine vehicles, much research effort has been devoted to this area during the past century. For example, the pioneering research work can be traced back to Wagner, 1932, and the vast research work is summarized in a series of review articles, see e.g., Chu and Abramson (1961), Faltinsen (2000), Faltinsen et al. (2004), Howison et al. (1991) and Mizoguchi and Tanizawa (1996). An analytical method to predict slamming pressure which considers a number of physical parameters was proposed by Stavovy and Chuang (1976), while Mei et al. (1999), Toyama (1993) and Zhao and Faltinsen (1993), among others, developed models to address 2-D water impact of general sections. Water impact with finite deadrise angles was investigated by Faltinsen (2002), Wu et al. (2004) and Yettou et al. (2007). Faltinsen and Chezhian (2005), Korobkin and Scolan (2006), Peseux et al. (2005), Scolan and Korobkin (2001), and Takagi (2004), among others, addressed three-dimensional (3D) slamming problems, while Korobkin (2007) and Oliver (2007) developed second-order Wagner theories. A concept of compliant hulls was proposed and developed by Vorus (2000, 2004) toward wave-impact reduction. We note that due to vast literature in this area, we

* Corresponding author. Present address: School of Aerospace, Xi'an Jiaotong University, Xi'an 710049, PR China. Tel.: +86 29 8266 8751; fax: +86 29 8266 9044.

E-mail addresses: zmqin@mail.xjtu.edu.cn (Z. Qin), rbatra@vt.edu (R.C. Batra).

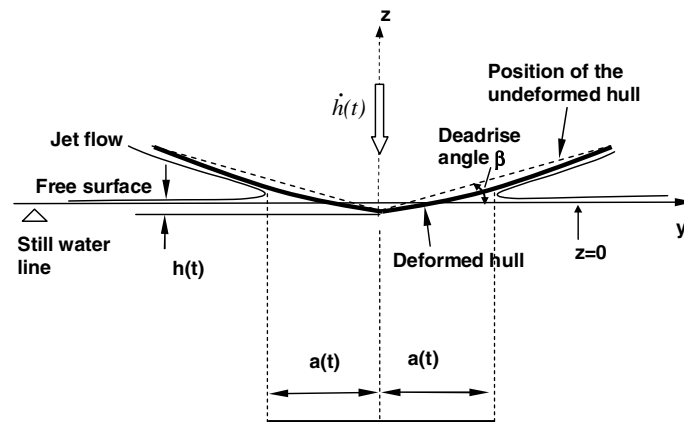


Fig. 1. Schematic sketch of the problem studied depicting slamming upon the bottom surface of a hull.

have listed only a few references. However, high complexities of the slamming phenomena require continuous research to improve upon and optimize hull's design. In this context, issues of hydroelastic effect during the slamming impact on structural deformations have drawn considerable attention, see e.g., Berezniński (2001), Faltinsen (1999), Khabakhpashva (2005), Korobkin (1995), Kvålsvold and Faltinsen (1995), and Scolan (2004).

This research effort becomes even more important in the design of impact-resistant marine hulls made of composite sandwich structures, mainly due to hydroelastic effect induced by the more prominent structural deformations during slamming impacts (Hayman, 1993).

We investigate here the local hydroelastic effects of slamming impact on a composite sandwich marine hull. More specifically, due to high-peak pressures developed during short-duration slamming impacts, hull's local deformations must be considered in a mathematical model of the problem. As proposed by Hohe and Librescu (2003), we use a higher-order transverse shear and transverse normal deformation theory for the core, and the Kirchhoff plate theory for the face sheets to simulate infinitesimal elastic deformations of a sandwich panel. In this theory, the in-plane displacement of the core is expanded up to third-order in the thickness coordinate, whereas a second-order expansion is used for the transverse displacement of the core. Following the name convention proposed by Barut et al. (2001), the theory is termed as {3,2}-order theory. A higher-order sandwich plate theory can be systematically developed based on a k th ($k = 0, 1, 2, \dots$) order plate theory of Batra et al. (2002) and Batra et al. (2002), in which both the transverse normal and transverse shear deformations are considered, and the three displacement components are expanded up to k th order in the thickness coordinate.

Recalling that the hydrodynamic load which accounts for hull's deformations is highly localized, the bottom slamming problem is idealized as that of a deformable sandwich wedge entering water with a uniform vertically downward speed (see Fig. 1). The system of nonlinear governing equations accounting for deformations of the hull and flow of the water, and the associated boundary conditions are derived by using the extended Hamilton's principle (Meirovitch (1997)). Here, the nonlinearity arises due to the a priori unknown length of the wetted surface which is a nonlinear function of hull's deformations. Also, deformations of the hull are to be determined by solving the governing equations. The solution of the problem necessitates the evaluation of singular integrals. An algorithm has been developed for numerically solving the system of coupled nonlinear equations. It has been verified by comparing the numerical solution with the analytical solution of a representative problem.

In order to validate the structural model, a general purpose finite element code, ABAQUS (2004), is used to compute natural frequencies of a dry sandwich panel. It is found that frequencies from the {3,2}-order theory agree well with those predicted by ABAQUS[®]. It is also found that the natural frequencies of the sandwich panel converge rapidly when mode shapes of the corresponding Euler–Bernoulli beam are taken as the basis functions. The mode shapes of the sandwich panel are expressed as polynomials in the axial coordinate and are used to reduce governing equations to a state-space form. Deformations of a sandwich panel due to hydrodynamic pressure have been studied, and the effect of the penetration speed of the hull into water has been delineated.

2. Formulation of the problem

Since we are considering the local slamming impact on a hull, the bottom slamming problem is idealized as a 2D (plane-strain) water entry of a deformable wedge (see Fig. 1). We use Lagrangian rectangular Cartesian coordinates (x_2, x_3) depicted in Fig. 2 to study deformations of the hull penetrating stationary water with a vertically downward speed $\dot{h}(t)$. Furthermore, the hull is comprised of a sandwich panel with relatively stiff top and bottom face sheets and a flexible core. Such a structure reduces weight without sacrificing hull's stiffness and resistance to impact loads. During the slamming process, hull's defor-

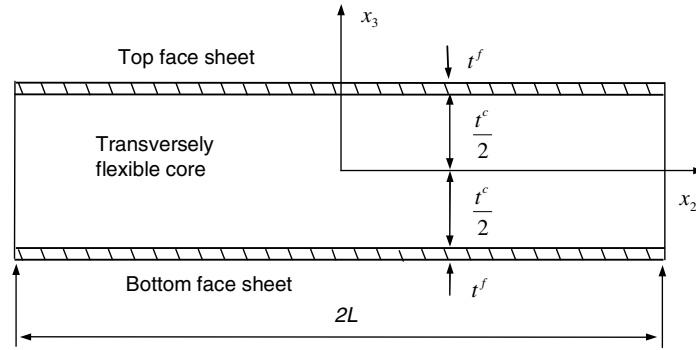


Fig. 2. Geometry of a sandwich panel.

mations are assumed to be infinitesimal, and symmetric about the x_3 -axis. It is thus tacitly assumed that the hull is symmetric about the x_3 -axis. Our analysis further rules out snap through instability of the wedge.

2.1. Deformations of the sandwich panel

For the sandwich panel shown in Fig. 2, we follow Hohe and Librescu (2003), and adopt the Kirchhoff hypothesis for the top and the bottom face sheets but consider transverse deformations of the core. We thus assume following expressions for the displacement field in the face sheets and the core.

- For the top and the bottom face sheets:

$$v_2^t = u_2^a + u_2^d - \left(x_3 - \frac{t^c + t^f}{2}\right)(u_{3,2}^a + u_{3,2}^d), \quad (1a)$$

$$v_2^b = u_2^a - u_2^d - \left(x_3 + \frac{t^c + t^f}{2}\right)(u_{3,2}^a - u_{3,2}^d), \quad (1b)$$

$$v_3^t = u_3^a + u_3^d, \quad v_3^b = u_3^a - u_3^d, \quad (1c)$$

where t^c and t^f equal, respectively, the thickness of the core and of the face sheet, and the two face sheets are of equal thickness. Superscripts a and d signify the average and the half-difference of the top and the bottom face sheets' mid-surface displacements u_j^t and u_j^b . That is,

$$u_j^a \equiv \frac{1}{2}(u_j^t + u_j^b), \quad u_j^d \equiv \frac{1}{2}(u_j^t - u_j^b), \quad j = 2, 3, \quad (2a)$$

and subscripts t and b imply the top and the bottom face sheets, also $u_{3,2} \equiv \partial u_3 / \partial x_2$. Note that u_2 and u_3 denote displacements in the x_2 and the x_3 directions of a point on the mid-surface, but v_2 and v_3 signify displacements of any point of the panel.

- For the core:

$$v_2^c = u_2^a + \frac{t^f}{2} u_{3,2}^d + \frac{2x_3}{t^c} u_2^d + \frac{t^f}{t^c} x_3 u_{3,2}^a + \left[\frac{4(x_3)^2}{(t^c)^2} - 1\right] \Phi_2^c + 2x_3 \left[\frac{4(x_3)^2}{(t^c)^2} - 1\right] \Omega_2^c, \quad (3a)$$

$$v_3^c = u_3^a + \frac{2x_3}{t^c} u_3^d + \left[\frac{4(x_3)^2}{(t^c)^2} - 1\right] \Phi_3^c, \quad (3b)$$

where displacement functions Φ_2^c , Ω_2^c and Φ_3^c describe the warping of the core, and superscripts f and c denote, respectively, the quantity for the face sheets and the core. The transverse shear strain in the core is a quadratic function of x_3 , and the transverse normal strain is a polynomial of degree one in x_3 . We note that Eqs. (2) and (3) involve seven functions, u_2^a , u_2^d , u_3^a , u_3^d , Φ_2^c , Ω_2^c and Φ_3^c , of the spatial variable x_2 . The displacement field at points on the interfaces between face sheets and the core is continuous.

2.2. Hydrodynamic pressure distribution during slamming impact

For studying the hydrodynamic problem, an Eulerian coordinate system yz which coincides with the Lagrangian coordinate system x_2x_3 at the beginning of penetration is used. We restrict ourselves to small disturbances in the flow, adopt a linear theory, and study deformations symmetric with respect to the z -axis. Since x_2 -displacement of

water except in the domain of jet flow is expected to be infinitesimal, we use coordinates x_2 and y interchangeably.

We assume that water is inviscid and incompressible, and the flow is irrotational (see e.g., Faltinsen, 1997; Mei et al., 1999; Zhao and Faltinsen, 1993). Thus potential functions can be used to derive the displacement and velocity fields in water. We also neglect gravitational force in the flow since fluid acceleration associated with the initial impact is much larger than that due to gravity. With Φ_h denoting the displacement potential of water, we get the following governing equations for Φ_h (see Fig. 1 for geometric specifications):

$$\frac{\partial^2 \Phi_h}{\partial y^2} + \frac{\partial^2 \Phi_h}{\partial z^2} = 0, \quad z < 0, \tag{4a}$$

$$\Phi_h = 0, \quad |y| > a(t), \quad z = 0^-, \tag{4b}$$

$$\frac{\partial \Phi_h}{\partial z} = -h(t) + f(y) + u_3^b(y, t), \quad |y| < a(t), \quad z = 0^-, \tag{4c}$$

$$\Phi_h \rightarrow 0, \quad y^2 + z^2 \rightarrow \infty, \tag{4d}$$

where $a(t)$ denotes the length of the right-half wetted hull, which is to be determined as a part of the solution of the problem. It is also the y -coordinate of the right side contact point of the hull with the free surface of water. In Eqs. (4c) and (4d), $h(t)$ equals the time-dependent penetration of hull's center into water, $z = f(y)$ describes the profile of the bottom surface of the hull, and $u_3^b(y, t)$ equals the vertical displacement of a point on the bottom surface of the hull. In writing Eq. (4c), we have assumed that there is no separation between the hull and the water. Thus the vertical displacement of a point on the bottom surface of the hull equals that of the contacting water particle.

In terms of the following non-dimensional variables

$$\tilde{y} \equiv \frac{y}{a(t)}, \quad \tilde{z} \equiv \frac{z}{a(t)}, \quad t > 0, \tag{5}$$

the wetted length is normalized to $(-1, 1)$.

In order to determine the displacement potential Φ_h , we distribute vortices of intensity γ_b on the wetted length $\tilde{y} \in (-1, 1)$, $z = 0$. The potential theory (see e.g., Katz and Plotkin, 1991) gives

$$\Phi_h(\tilde{y}, \tilde{z}, t) = \frac{1}{2\pi} \int_{-1}^1 \gamma_b(\tilde{y}_0, t) \tan^{-1} \frac{\tilde{z}}{\tilde{y} - \tilde{y}_0} d\tilde{y}_0, \quad \tilde{z} < 0. \tag{6}$$

Fulfillment of boundary condition (4c) yields the following Cauchy type singular integral equation:

$$\frac{1}{2\pi} \int_{-1}^1 \frac{\gamma_b(\tilde{y}_0, t)}{\tilde{y} - \tilde{y}_0} d\tilde{y}_0 = a(t) \{h(t) - f[a(t)|\tilde{y}|] - u_3^b[|\tilde{y}|a(t), t]\} \equiv \kappa[a(t)|\tilde{y}|, t]. \tag{7}$$

Here, $|\cdot|$ is the absolute value operator.

Since the water flow across end points $\tilde{y} = \pm 1$ in the horizontal direction must be bounded in amplitude, the solvability condition for Eq. (7) is (Gakhov, 1966)

$$\int_{-1}^1 \frac{\kappa[a(t)|\tilde{y}_0|, t]}{\sqrt{1 - \tilde{y}_0^2}} d\tilde{y}_0 = 0. \tag{8}$$

Eq. (8) is called the Wagner condition (Scolan and Korobkin, 2001), and is used to determine the unknown contact point $a(t)$ which depends on the penetration depth $h(t)$, shape $z = f(y)$ of the wetted hull surface, and hull's deformation u_3^b .

The solution of Eq. (7) can be written as (Gakhov, 1966)

$$\gamma_b(\tilde{y}, t) = -\frac{\sqrt{1 - \tilde{y}^2}}{\pi} \int_{-1}^1 \frac{\kappa[a(t)|\tilde{y}_0|, t] d\tilde{y}_0}{\sqrt{1 - \tilde{y}_0^2}(\tilde{y} - \tilde{y}_0)}, \quad |\tilde{y}| < 1. \tag{9}$$

Once the vortex intensity γ_b has been obtained from Eq. (9), the displacement potential Φ_h can be determined from Eq. (6). As a result, the non-dimensional elevation of the free surface of water can be deduced from

$$\eta(\tilde{y}, t) = \left. \frac{\partial \Phi_h}{\partial z} \right|_{z=0^-} = -\frac{1}{2\pi} \int_{-1}^1 \frac{\gamma_b(\tilde{y}_0, t)}{\tilde{y} - \tilde{y}_0} d\tilde{y}_0, \quad |\tilde{y}| > 1. \tag{10}$$

The distribution of the hydrodynamic pressure, $p_s(\tilde{y}, t)$, on the wetted hull surface is given by

$$p_s(\tilde{y}, t) = \begin{cases} \rho_h \frac{\partial^2 \Phi_h(\tilde{y}, 0^-, t)}{\partial t^2}, & |\tilde{y}| < 1, \\ 0, & |\tilde{y}| > 1, \end{cases} \tag{11}$$

in which ρ_h is the mass density of water, and the contribution from the quadratic term in Bernoulli's equation $(1/2)(\partial \nabla \Phi_h / \partial t) \cdot (\partial \nabla \Phi_h / \partial t)$ has been neglected.

2.3. Governing equations

Since the problem has been assumed to be symmetric about the z -axis, we study deformations of the hull and the water occupying the region $L \geq y \geq 0$, where L is the length of the hull (see Fig. 2).

The governing equations and the pertinent boundary conditions for the hull can be derived by using the extended Hamilton's principle (Meirovitch, 1997):

$$\int_{t_1}^{t_2} (\delta \mathcal{T} - \delta \mathcal{U} + \overline{\delta W}_e) dt = 0, \quad (12a)$$

with

$$\delta u_j^a = \delta u_j^d = \delta \Phi_j^c = \delta \Omega_2^c = 0 \quad \text{at } t = t_1 \text{ and } t_2, \quad (12b)$$

where $j = 2, 3$, $\delta \mathcal{T}$ and $\delta \mathcal{U}$ denote the virtual kinetic and the virtual strain energies, respectively, while $\overline{\delta W}_e$ denotes the virtual work done by external forces. For the present problem, expressions for $\delta \mathcal{T}$, $\delta \mathcal{U}$ and $\overline{\delta W}_e$ are given below.

- *Virtual kinetic energy:*

$$\delta \mathcal{T} = \int_0^L \left\{ \int_{t^c/2}^{t^c/2+t^f} \rho^f (\dot{v}_2^t \delta \dot{v}_2^t + \dot{v}_3^t \delta \dot{v}_3^t) dx_3 + \int_{-t^c/2}^{t^c/2} \rho^c \dot{v}_3^c \delta \dot{v}_3^c dx_3 + \int_{-t^c/2-t^f}^{-t^c/2} \rho^f (\dot{v}_2^b \delta \dot{v}_2^b + \dot{v}_3^b \delta \dot{v}_3^b) dx_3 \right\} dx_2. \quad (13)$$

- *Virtual strain energy:*

$$\delta \mathcal{U} = \int_{V.H.} \sigma_{ij} \delta \epsilon_{ij} dV = \int_0^L \left\{ \int_{t^c/2}^{t^c/2+t^f} \sigma_{22}^t \delta \epsilon_{22}^t dx_3 + \int_{-t^c/2-t^f}^{-t^c/2} \sigma_{22}^b \delta \epsilon_{22}^b dx_3 + \int_{-t^c/2}^{t^c/2} (\sigma_{33}^c \delta \epsilon_{33}^c + \sigma_{23}^c \delta \gamma_{23}^c) dx_3 \right\} dx_2. \quad (14)$$

Here, ρ^f and ρ^c are mass densities of the face sheets and the core, respectively, and $V.H.$ in Eq. (14) denotes the volume initially occupied by the right-half wedge. It is noted that the virtual kinetic energy density $\rho^c \dot{v}_2^c \delta \dot{v}_2^c$ and the virtual strain energy density $\sigma_{22}^c \delta \epsilon_{22}^c$ are disregarded due to the adoption of weak core (Hohe and Librescu, 2003).

- *Virtual work due to external forces:*

$$\overline{\delta W}_e = \int_0^{a(t)} p_s(\tilde{y}(y), t) \delta u_3^b dy. \quad (15)$$

Here, $\overline{\delta W}_e$ equals the work done by the hydrodynamic pressure $p_s(\tilde{y}, t)$ in deforming the hull. We note that $p_s(\tilde{y}(y), t)$ accounts for the interaction between deformations of the hull and the water underneath it.

We write equations of motion and the associated boundary conditions in terms of the following stress resultants and couples.

$$(N_{22}^t, M_{22}^t) \equiv \int_{t^c/2}^{t^c/2+t^f} (1, x_3) \sigma_{22}^t dx_3, \quad (16a)$$

$$(N_{22}^b, M_{22}^b) \equiv \int_{-t^c/2-t^f}^{-t^c/2} (1, x_3) \sigma_{22}^b dx_3, \quad (16b)$$

$$(N_{33}^c, M_{33}^c) \equiv \int_{-t^c/2}^{t^c/2} (1, x_3) \sigma_{33}^c dx_3, \quad (16c)$$

$$(N_{23}^c, M_{23}^c, L_{23}^c) \equiv \int_{-t^c/2}^{t^c/2} (1, x_3, (x_3)^2) \sigma_{23}^c dx_3. \quad (16d)$$

The governing equations associated with variations in different variables are:

$$\delta u_2^a: N_{22,2}^a - m_0^f \ddot{u}_2^a = 0, \quad (17a)$$

$$\delta u_2^d: N_{22,2}^d - \frac{1}{t^c} N_{23}^c - m_0^f \ddot{u}_2^d = 0, \quad (17b)$$

$$\delta \Phi_2^c: M_{23}^c = 0, \quad (17c)$$

$$\delta \Omega_2^c: -N_{23}^c + \frac{12}{(t^c)^2} L_{23}^c = 0, \quad (17d)$$

$$\delta u_3^a: -(2m_0^f + m_0^c) \ddot{u}_3^a - m_2^c \ddot{\Phi}_3^c + 2q_3^a + 2M_{22,22}^a + \left(1 + \frac{t^f}{t^c}\right) N_{23,2}^c = 0, \quad (17e)$$

$$\delta u_3^d: -(2m_0^f + m_0^c + m_2^c) \ddot{u}_3^d - m_2^c \ddot{\Phi}_3^c + 2q_3^d + 2M_{22,22}^d - \frac{2}{t^c} N_{33}^c = 0, \quad (17f)$$

$$\delta \Phi_3^c: -m_2^c \ddot{u}_3^a - m_4^c \ddot{\Phi}_3^c - \frac{8}{(t^c)^2} M_{33}^c - N_{23,2}^c + \frac{4}{(t^c)^2} L_{23,2}^c = 0. \quad (17g)$$

In Eqs. (17a)–(17g), m_0^f , m_0^c , m_2^c , and m_4^c are inertial coefficients, and their expressions are listed in Eqs. (B.2a–d) of Appendix B. In Eqs. (17e) and (17f), q_3^a and q_3^d are defined as:

$$q_3^a = \frac{q_3^t + q_3^b}{2} = \frac{1}{2} p_s(y, t), \quad q_3^d = \frac{q_3^t - q_3^b}{2} = -\frac{1}{2} p_s(y, t). \tag{18}$$

The corresponding boundary conditions at $x_2 = 0, L$ are:

$$\delta u_2^a : N_{22}^a = 0 \text{ or } u_2^a = \hat{u}_2^a, \tag{19a}$$

$$\delta u_2^d : N_{22}^d = 0 \text{ or } u_2^d = \hat{u}_2^d, \tag{19b}$$

$$\delta u_3^a : 2M_{22,2}^a + \left(1 + \frac{t^f}{t^c}\right) N_{23}^c = 0 \text{ or } u_3^a = \hat{u}_3^a, \tag{19c}$$

$$\delta u_3^d : M_{22,2}^d + \frac{1}{t^c} M_{23}^c = 0 \text{ or } u_3^d = \hat{u}_3^d, \tag{19d}$$

$$\delta \Phi_3^c : \frac{4}{(t^c)^2} L_{23}^c - N_{23}^c = 0 \text{ or } \Phi_3^c = \hat{\Phi}_3^c, \tag{19e}$$

$$\delta u_{3,2}^a : M_{22}^a = 0 \text{ or } u_{3,2}^a = \hat{u}_{3,2}^a, \tag{19f}$$

$$\delta u_{3,2}^d : M_{22}^d = 0 \text{ or } u_{3,2}^d = \hat{u}_{3,2}^d, \tag{19g}$$

in which, quantities with a superimposed hat are specified at the boundaries. In the sequel, we focus on face sheets and the core comprised of homogeneous and orthotropic materials with the axes of orthotropy coincident with the axes (x_2, x_3) of the rectangular Cartesian coordinate system. For simplicity, we consider the case in which the top and the bottom face sheets are made of the same homogeneous and orthotropic material, and the lay-ups are identical and symmetric with respect to their individual mid-surfaces. Constitutive equations for the stress resultants and couples defined in Eqs. (16a)–(16d) can be written as

$$N_{22}^a = A_{22}^f u_{2,2}^a, \quad N_{22}^d = A_{22}^f u_{2,2}^d, \quad M_{22}^a = -D_{22}^f u_{3,2,2}^a, \tag{20a-c}$$

$$M_{22}^d = -D_{22}^f u_{3,2,2}^d, \quad N_{33}^c = \frac{2}{t^c} A_{33}^c u_3^d, \quad M_{33}^c = \frac{8}{(t^c)^2} D_{33}^c \Phi_3^c, \tag{20d-f}$$

$$N_{23}^c = \frac{2}{t^c} A_{23}^c u_2^d + \left(1 + \frac{t^f}{t^c}\right) A_{23}^c u_{3,2}^a + \left[\frac{24}{(t^c)^2} D_{23}^c - 2A_{23}^c\right] \Omega_2^c + \left[\frac{4}{(t^c)^2} D_{23}^c - A_{23}^c\right] \Phi_{3,2}^c,$$

$$M_{23}^c = \frac{8}{(t^c)^2} D_{23}^c \Phi_2^c + \frac{2}{t^c} D_{23}^c u_{3,2}^d, \tag{20g}$$

$$M_{23}^c = \frac{8}{(t^c)^2} D_{23}^c \Phi_2^c + \frac{2}{t^c} D_{23}^c u_{3,2}^d, \tag{20h}$$

$$L_{23}^c = \frac{2}{t^c} D_{23}^c u_2^d + \left(1 + \frac{t^f}{t^c}\right) D_{23}^c u_{3,2}^a + \left[\frac{F_{23}^c}{(t^c)^2} - 2D_{23}^c\right] \Omega_2^c + \left[\frac{4F_{23}^c}{(t^c)^2} - D_{23}^c\right] \Phi_{3,2}^c. \tag{20i}$$

Here A_{22}^f, D_{22}^f , etc. are stiffnesses that equal integrals over the thickness of moments of different orders with respect to the x_2 -axis of material elasticities; their expressions are given in Eqs. (B.6a-g). It is noted that in Eqs. (19a)–(19e), there is no boundary condition for Φ_2^c and Ω_2^c since we have neglected in Eq. (14) the strain energy due to axial deformations of the core. Furthermore, because the kinetic energy due to axial displacements of the core particles has been neglected, no time derivatives of Φ_2^c and Ω_2^c appear in Eqs. (17c) and (17d).

Based on Eqs. (17c) and (17d), and 20g, 20h and 20i, the following kinematic relations are obtained:

$$\Phi_2^c = -\frac{t^c}{4} u_{3,2}^d, \quad \Omega_2^c = \mathcal{R}_1 u_2^d + \mathcal{R}_2 u_{3,2}^a + \mathcal{R}_3 \Phi_{3,2}^c, \tag{21a, b}$$

where

$$\mathcal{R}_1 \equiv \frac{1}{\mathcal{R}_d} \left[\frac{2}{t^c} A_{23}^c - \frac{24}{(t^c)^3} D_{23}^c \right], \quad \mathcal{R}_2 \equiv \frac{1}{\mathcal{R}_d} \left(1 + \frac{t^f}{t^c} \right) \left[A_{23}^c - \frac{12}{(t^c)^2} D_{23}^c \right], \tag{22a, b}$$

$$\mathcal{R}_3 \equiv \frac{1}{\mathcal{R}_d} \left[\frac{16D_{23}^c}{(t^c)^2} - A_{23}^c - \frac{48F_{23}^c}{(t^c)^4} \right], \quad \mathcal{R}_d \equiv \frac{12F_{23}^c}{(t^c)^4} - \frac{48D_{23}^c}{(t^c)^2} + 2A_{23}^c, \tag{22c, d}$$

with \mathcal{R}_d being assumed to be different from zero.

Eqs. (21a,b) reduce the number of unknowns in Eqs. (17a)–(17g) from 7 to 5 (i.e., $u_2^a, u_2^d, u_3^a, u_3^d, \Phi_3^c$). We note that Eqs. (17a), (19a) and (20a) involve only u_2^a . Hence, they can be solved for u_2^a without considering the remaining governing equations. For the case when the wedge's initial conditions are $u_2^a(x_2, t = 0) = 0$ and $\dot{u}_2^a(x_2, t = 0) = 0$, then $u_2^a(x_2, t) \equiv 0$ during the entire

slamming impact. In the sequel, we adopt these initial conditions for u_2^d . Thus, the basic unknowns reduce to four, i.e., u_2^d , u_3^d , u_3^c and ϕ_3^c , which are to be determined by simultaneously solving Eqs. (17b) and 17e, 17f, 17g under appropriate initial and boundary conditions.

Substitution from Eqs. (21a,b) into Eqs. (17e)–(17g) gives the following governing equations for u_2^d , u_3^d , u_3^c and ϕ_3^c .

$$\begin{aligned} & (t^c A_{22}^a) u_{2,22}^d - \left[\frac{2}{t^c} A_{23}^c + \left(\frac{24D_{23}^c}{(t^c)^2} - 2A_{23}^c \right) \mathcal{R}_1 \right] u_2^d \\ & - \left[\left(1 + \frac{t^f}{t^c} \right) A_{23}^c + \left(\frac{24D_{23}^c}{(t^c)^2} - 2A_{23}^c \right) \mathcal{R}_2 \right] u_{3,2}^d \\ & - \left[\left(\frac{24D_{23}^c}{(t^c)^2} - 2A_{23}^c \right) \mathcal{R}_3 + \left(\frac{4D_{23}^c}{(t^c)^2} - A_{23}^c \right) \right] \phi_{3,2}^c - (m_0^f t^c) \ddot{u}_2^d = 0, \end{aligned} \tag{23a}$$

$$\begin{aligned} & - (2m_0^f + m_0^c) \ddot{u}_3^d - m_2^c \ddot{\phi}_3^c + 2q_3^d - 2D_{22}^f u_{3,2222}^d \\ & + \left(1 + \frac{t^f}{t^c} \right) \left[\frac{2}{t^c} A_{23}^c + \left(\frac{24D_{23}^c}{(t^c)^2} - 2A_{23}^c \right) \mathcal{R}_1 \right] u_{2,2}^d \\ & + \left(1 + \frac{t^f}{t^c} \right) \left[\left(1 + \frac{t^f}{t^c} \right) A_{23}^c + \left(\frac{24D_{23}^c}{(t^c)^2} - 2A_{23}^c \right) \mathcal{R}_2 \right] u_{3,22}^d \\ & + \left(1 + \frac{t^f}{t^c} \right) \left[\left(\frac{24D_{23}^c}{(t^c)^2} - 2A_{23}^c \right) \mathcal{R}_3 + \left(\frac{4D_{23}^c}{(t^c)^2} - A_{23}^c \right) \right] \phi_{3,22}^c = 0, \end{aligned} \tag{23b}$$

$$\begin{aligned} & - (2m_0^f + m_2^c + m_0^c) \ddot{u}_3^d - m_2^c \ddot{\phi}_3^c + 2q_3^d - 2D_{22}^f u_{3,2222}^d - \frac{4A_{33}^c}{(t^c)^2} u_3^d = 0, \\ & - (m_2^c \ddot{u}_3^d + m_4^c \ddot{\phi}_3^c) - \frac{64D_{33}^c}{(t^c)^4} \phi_3^c - \frac{2}{3} \left[\frac{2A_{23}^c}{t^c} + \left(\frac{24D_{23}^c}{(t^c)^2} - 2A_{23}^c \right) \mathcal{R}_1 \right] u_{2,2}^d \end{aligned} \tag{23c}$$

$$\begin{aligned} & - \frac{2}{3} \left[\left(1 + \frac{t^f}{t^c} \right) A_{23}^c + \left(\frac{24D_{23}^c}{(t^c)^2} - 2A_{23}^c \right) \mathcal{R}_2 \right] u_{3,22}^d \\ & - \frac{2}{3} \left[\left(\frac{24D_{23}^c}{(t^c)^2} - 2A_{23}^c \right) \mathcal{R}_3 + \left(\frac{4D_{23}^c}{(t^c)^2} - A_{23}^c \right) \right] \phi_{3,22}^c = 0. \end{aligned} \tag{23d}$$

Eqs. (23a)–(23d) are to be supplemented with values of functions $u_2^d(x_2, 0)$, $\dot{u}_2^d(x_2, 0)$, $u_3^d(x_2, 0)$, $\dot{u}_3^d(x_2, 0)$, $\phi_3^c(x_2, 0)$, $\dot{\phi}_3^c(x_2, 0)$, $u_3^d(x_2, 0)$, and $\dot{u}_3^d(x_2, 0)$, which form initial conditions for the problem.

3. Solution

3.1. State-space formulation of the problem

An interesting feature of the above formulated problem is that even though the structural and the hydrodynamic problems by themselves are linear, the coupled one is nonlinear because the unknown contact point $a(t)$ is a nonlinear function of deformations u_3^d and u_3^c , and deformations u_2^d , u_3^d and ϕ_3^c depend on $a(t)$. We solve the nonlinear problem numerically by the Extended Galerkin's method (EGM) (see e.g., Librescu et al., 1997; Palazzotto and Linnemann, 1991) for the structural part, and the fourth-order Runge-Kutta method for the hydrodynamic part.

We spatially semi-discretize the structural part of the governing Eqs. (23a)–(23c), rewrite the Wagner condition (8) in a differential form (Korobkin, 1995), cast these differential equations in the state-space form, and assume the following essential boundary and initial conditions:

$$u_3^d(0, t) = u_3^c(0, t) = u_{3,2}^d(0, t) = u_{3,2}^c(0, t) = u_2^d(0, t) = \phi_3^c(0, t) = 0, \tag{24a}$$

$$u_3^d(L, t) = u_3^c(L, t) = u_{3,2}^d(L, t) = u_{3,2}^c(L, t) = u_2^d(L, t) = \phi_3^c(L, t) = 0, \tag{24b}$$

$$u_3^d(x_2, 0) = u_3^c(x_2, 0) = u_2^d(x_2, 0) = \phi_3^c(x_2, 0) = 0. \tag{24c}$$

We approximate the four unknown functions as follows:

$$u_2^d(y, t) \approx \Psi_2^T(y) \mathbf{x}_2(t), \quad u_3^d(y, t) \approx \Psi_a^T(y) \mathbf{x}_a(t), \tag{25a, b}$$

$$u_3^c(y, t) \approx \Psi_d^T(y) \mathbf{x}_d(t), \quad \phi_3^c(y, t) \approx \Psi_w^T(y) \mathbf{x}_w(t), \tag{25c, d}$$

in which Ψ_2 , Ψ_a , Ψ_d and Ψ_w are vectors of basis functions, while \mathbf{x}_2 , \mathbf{x}_a , \mathbf{x}_d and \mathbf{x}_w are vectors of generalized coordinates. In order to identically satisfy boundary conditions (24a) and (24b), the following basis functions are used.

$$\Psi_a(y) = \Psi_d(y) = \{W_1(y), W_2(y), \dots, W_{N_s}(y)\}^T, \tag{26a}$$

$$\Psi_2(y) = \Psi_w(y) = \left\{ \sin \frac{\pi y}{L}, \sin \frac{2\pi y}{L}, \dots, \sin \frac{N_s \pi y}{L} \right\}^T. \tag{26b}$$

Here N_s denotes the number of basis functions, and W_i is the normalized i th eigenmode ($i = \overline{1, N_s}$) of a clamped–clamped Euler–Bernoulli beam defined as

$$W_i(y) = \frac{W_i^0(y)}{\sqrt{\int_0^L [W_i^0(y)]^2 dy}} \tag{27}$$

with

$$W_i^0(y) = \left[\sin \left(\hat{\beta}_i \frac{y}{L} \right) - \sinh \left(\hat{\beta}_i \frac{y}{L} \right) \right] - \frac{\sin \hat{\beta}_i - \sinh \hat{\beta}_i}{\cos \hat{\beta}_i - \cosh \hat{\beta}_i} \left[\cos \left(\hat{\beta}_i \frac{y}{L} \right) - \cosh \left(\hat{\beta}_i \frac{y}{L} \right) \right], \tag{28}$$

and $\hat{\beta}_i$ is the positive i th root of the equation $\cos \hat{\beta} \cosh \hat{\beta} - 1 = 0$.

In terms of the representation (25b,c) of u_3^a and u_3^d , the displacement u_3^b of the bottom face sheet can be written as

$$u_3^b(y, t) = u_3^a(y, t) - u_3^d(y, t) = \Psi_a^T(y) \mathbf{x}_a(t) - \Psi_d^T(y) \mathbf{x}_d(t). \tag{29}$$

In order to evaluate the singular integral in Eq. (9) which involves u_3^b (cf. Eq. (7)) and hence basis functions $\Psi_a(y)$ and $\Psi_d(y)$, we approximate these basis functions by polynomials. This is accomplished via the curve-fitting utility in Mathematica 6 (Wolfram Research, Inc, 2007), and the polynomials are listed in Eqs. (B.7a,b). The key step in evaluating the singular integral in Eq. (9) is the evaluation of the following two integrals:

$$\hat{I}_k(\tilde{y}) \equiv \int_0^1 \frac{\tilde{y}_0^k}{\sqrt{1 - \tilde{y}_0^2}(\tilde{y}_0 - \tilde{y})} d\tilde{y}_0, \tag{30a}$$

$$I_k(\tilde{y}) \equiv \int_{-1}^1 \frac{|\tilde{y}_0|^k}{\sqrt{1 - \tilde{y}_0^2}(\tilde{y}_0 - \tilde{y})} d\tilde{y}_0 = \hat{I}_k(\tilde{y}) - \hat{I}_k(-\tilde{y}), \tag{30b}$$

where k is a nonnegative integer.

By using the Hilbert transform (Erdélyi et al., 1954) and the following recurrence relation

$$\hat{I}_{k+1}(\tilde{y}) = \tilde{y} \hat{I}_k(\tilde{y}) + \int_0^1 \frac{\tilde{y}_0^k}{\sqrt{1 - \tilde{y}_0^2}} d\tilde{y}_0, \tag{31}$$

integrals in Eqs. (30a) and (30b) can be evaluated for all desired values of k ; values of I_0, I_1, \dots, I_{16} are listed in Appendix A.

Omitting details of deriving the Galerkin approximation of a set of partial differential equations, we write governing Eqs. (23a)–(23d) in the following form:

$$\begin{bmatrix} \mathbf{M}_{22}^s & \mathbf{0} & \mathbf{0} & \mathbf{0} \\ \mathbf{0} & \mathbf{M}_{aa}^s + \mathbf{M}_{aa}^h & \mathbf{M}_{ad}^h & \mathbf{M}_{aw}^s \\ \mathbf{0} & \mathbf{M}_{da}^h & \mathbf{M}_{dd}^s + \mathbf{M}_{dd}^h & \mathbf{M}_{dw}^s \\ \mathbf{0} & \mathbf{M}_{wa}^s & \mathbf{0} & \mathbf{M}_{ww}^s \end{bmatrix} \begin{Bmatrix} \ddot{\mathbf{x}}_2 \\ \ddot{\mathbf{x}}_a \\ \ddot{\mathbf{x}}_d \\ \ddot{\mathbf{x}}_w \end{Bmatrix} + \begin{bmatrix} \mathbf{0} & \mathbf{0} & \mathbf{0} & \mathbf{0} \\ \mathbf{0} & \mathbf{C}_{aa}^h & \mathbf{C}_{ad}^h & \mathbf{0} \\ \mathbf{0} & \mathbf{C}_{da}^h & \mathbf{C}_{dd}^h & \mathbf{0} \\ \mathbf{0} & \mathbf{0} & \mathbf{0} & \mathbf{0} \end{bmatrix} \begin{Bmatrix} \dot{\mathbf{x}}_2 \\ \dot{\mathbf{x}}_a \\ \dot{\mathbf{x}}_d \\ \dot{\mathbf{x}}_w \end{Bmatrix} + \begin{bmatrix} \mathbf{K}_{22}^s & \mathbf{K}_{2a}^s & \mathbf{0} & \mathbf{K}_{2w}^s \\ \mathbf{K}_{a2}^s & \mathbf{K}_{aa}^s + \mathbf{K}_{aa}^h & \mathbf{K}_{ad}^h & \mathbf{K}_{aw}^s \\ \mathbf{0} & \mathbf{K}_{da}^h & \mathbf{K}_{dd}^s + \mathbf{K}_{dd}^h & \mathbf{0} \\ \mathbf{K}_{w2}^s & \mathbf{K}_{wa}^s & \mathbf{0} & \mathbf{K}_{ww}^s \end{bmatrix} \begin{Bmatrix} \mathbf{x}_2 \\ \mathbf{x}_a \\ \mathbf{x}_d \\ \mathbf{x}_w \end{Bmatrix} = \begin{Bmatrix} \mathbf{0} \\ -\mathbf{E}_{aa}^h \mathbf{c}_b \\ -\mathbf{E}_{dd}^h \mathbf{c}_b \\ \mathbf{0} \end{Bmatrix} \tag{32}$$

where superscripts h and s denote, respectively, quantities associated with the hydrodynamic and the structural parts. Matrices $\mathbf{M}_{aa}^h, \mathbf{M}_{ad}^h, \mathbf{M}_{da}^h$ and \mathbf{M}_{dd}^h are referred to as added-mass matrices, and they depend upon $a(t)$; $\mathbf{C}_{aa}^h, \mathbf{C}_{ad}^h, \mathbf{C}_{da}^h$ and \mathbf{C}_{dd}^h are referred to as added-damping matrices, and they depend upon both $a(t)$ and $\dot{a}(t)$; while $\mathbf{K}_{aa}^h, \mathbf{K}_{ad}^h, \mathbf{K}_{da}^h$ and \mathbf{K}_{dd}^h are referred to as added-stiffness matrices, and they depend upon $a(t), \dot{a}(t)$ and $\ddot{a}(t)$. Matrices \mathbf{E}_{aa}^h and \mathbf{E}_{dd}^h on the right hand side of Eq. (32) also depend on $a(t), \dot{a}(t)$ and $\ddot{a}(t)$, and \mathbf{c}_b is a constant vector that defines the hull profile. Expressions for matrices with superscripts s, h and the vector \mathbf{c}_b are given, respectively, by Eqs. (B.1a-g), (B.3a-j) and (B.10a-o). Recall that $a(t)$ equals the wetted length and is to be determined as a part of the solution of the problem.

The state-space representation of Eq. (32) is

$$\dot{\mathbf{x}}(t) = \mathcal{A}(t) \mathbf{x}(t) + \mathbf{Q}(t) \tag{33}$$

with $\mathbf{x} = \{\mathbf{x}_2, \mathbf{x}_a, \mathbf{x}_d, \mathbf{x}_w, \dot{\mathbf{x}}_2, \dot{\mathbf{x}}_a, \dot{\mathbf{x}}_d, \dot{\mathbf{x}}_w\}^T$.

From Eq. (8), and following the approach of Korobkin (1995), the differential equation which governs the wetted length $a(t)$ is obtained as

$$\dot{a}(t) = \frac{\Gamma_n(t)}{\Gamma_d(t)}, \tag{34}$$

in which

$$\Gamma_n(t) \equiv \frac{\pi}{2} \dot{h}(t) - \frac{1}{2} \{ \Gamma_{n1}[a(t)] \dot{\mathbf{x}}_a(t) + \Gamma_{n2}[a(t)] \dot{\mathbf{x}}_d(t) \}, \quad (35a)$$

$$\Gamma_d(t) \equiv \Gamma_{d0}[a(t)] + \frac{1}{2} \{ \Gamma_{d1}[a(t)] \mathbf{x}_a(t) + \Gamma_{d2}[a(t)] \mathbf{x}_d(t) \}, \quad (35b)$$

$$\{ \Gamma_{n1}[a(t)], \Gamma_{n2}[a(t)] \} \equiv \int_0^{\pi/2} \{ \Psi_a^T(a(t) \sin \theta), \Psi_d^T(a(t) \sin \theta) \} d\theta, \quad (36)$$

and

$$\{ \Gamma_{d0}[a(t)], \Gamma_{d1}[a(t)], \Gamma_{d2}[a(t)] \} \equiv \int_0^{\pi/2} \left\{ \frac{df(c)}{dc}, \frac{d\Psi_a^T(c)}{dc}, \frac{d\Psi_d^T(c)}{dc} \right\} \Big|_{c=a(t) \sin \theta} d\theta. \quad (37)$$

When the right hand side of Eq. (34) goes to infinity, bow flare-type slamming occurs (Korobkin, 1995).

In terms of solutions of Eqs. (33) and (34), the hydrodynamic pressure distribution on the wetted hull's surface can be represented as

$$p_s(y, t) = \left(-\frac{\rho h}{\pi} \right) \left[\underbrace{c_b^T \{ \ddot{u}_j(y, t) \}}_{\text{un-deformed hull}} + \underbrace{\{ \ddot{u}^a(y, t) \}^T \mathbf{x}_a(t)}_{\text{hull's deformations}} + 2 \underbrace{\{ \ddot{u}^a(y, t) \}^T \dot{\mathbf{x}}_a(t)}_{\text{hull's deformations}} \right. \\ \left. + \underbrace{\{ \ddot{u}^a(y, t) \}^T \ddot{\mathbf{x}}_a(t)}_{\text{hull's deformations}} - \underbrace{\{ \ddot{u}^d(y, t) \}^T \mathbf{x}_d(t)}_{\text{hull's deformations}} - 2 \underbrace{\{ \ddot{u}^d(y, t) \}^T \dot{\mathbf{x}}_d(t)}_{\text{hull's deformations}} - \underbrace{\{ \ddot{u}^d(y, t) \}^T \ddot{\mathbf{x}}_d(t)}_{\text{hull's deformations}} \right], \quad (38)$$

in which a superimposed dot indicates partial differentiation with respect to time, and vectors $\{II\}$, $\{III^a\}$, $\{III^d\}$ are defined in Eqs. (B.9a–c). Term underlined by the single solid line on the right hand side of Eq. (38) denotes contribution from the un-deformed hull, while terms underlined by the wavy lines represent contributions from the hull's deformations.

During slamming impact, the total hydrodynamic load $P_0(t)$ at time t , per unit length (in the x or x_1 -direction) of the hull, is given by

$$P_0(t) \equiv \int_0^{a(t)} p_s(y, t) dy. \quad (39)$$

Similar to the stress intensity factor at a crack tip, we define the following slamming pressure intensity factor

$$\text{PIF}(t) = \lim_{y \rightarrow a^-(t)} p_s(y, t) \sqrt{a^2(t) - y^2}, \quad (40)$$

which is a measure of the peak pressure at the extremity of the wetted length.

3.2. Solution procedure and associated numerical issues

The solution can not be simply obtained by combining Eqs. (32) or (33) and (34) because the added-stiffness matrices \mathbf{K}_{aa}^h , \mathbf{K}_{ad}^h and \mathbf{K}_{dd}^h , and matrices \mathbf{E}_{aa}^h and \mathbf{E}_{dd}^h in Eq. (32) depend on $\ddot{a}(t)$, which in turn depends on $\ddot{\mathbf{x}}_a$ and $\ddot{\mathbf{x}}_d$ (see Eq. (34)). We use the central-difference method to estimate $\ddot{a}(t)$. That is,

$$\ddot{a}[t_k] = \frac{a[t_{k-1}] - 2a[t_k] + a[t_{k+1}]}{\Delta t^2}, \quad k \geq 1, \quad (41)$$

where Δt is the time step size, and $t_k = k\Delta t$. We take Δt to be a constant.

Differentiation with respect to time t of both sides of Eq. (34) gives

$$\ddot{a}(t) = \frac{\dot{\Gamma}_n(t)}{\Gamma_d(t)} - \frac{\dot{\Gamma}_d(t)}{\Gamma_d(t)} \dot{a}(t), \quad (42)$$

where based on Eqs. (35a) and (35b), $\dot{\Gamma}_n(t)$ and $\dot{\Gamma}_d(t)$ are given by

$$\dot{\Gamma}_n(t) = \frac{\pi}{2} \ddot{h}(t) - \left[\int_0^{\pi/2} \frac{d\Psi_a^T(c)}{dc} \Big|_{c=a(t) \sin \theta} d\theta \right] \dot{a}(t) \dot{\mathbf{x}}_a(t) + \left[\int_0^{\pi/2} \frac{d\Psi_d^T(c)}{dc} \Big|_{c=a(t) \sin \theta} d\theta \right] \dot{a}(t) \dot{\mathbf{x}}_d(t) \\ - \left[\int_0^{\pi/2} \Psi_a^T(a(t) \sin \theta) d\theta \right] \ddot{\mathbf{x}}_a(t) + \left[\int_0^{\pi/2} \Psi_d^T(a(t) \sin \theta) d\theta \right] \ddot{\mathbf{x}}_d(t), \quad (43a)$$

$$\dot{\Gamma}_d(t) = \left\{ \int_0^{\pi/2} \frac{d^2 f(c)}{dc^2} \Big|_{c=a(t) \sin \theta} \sin^2 \theta d\theta + \left[\int_0^{\pi/2} \frac{d^2 \Psi_a^T(c)}{dc^2} \Big|_{c=a(t) \sin \theta} \sin^2 \theta d\theta \right] \mathbf{x}_a(t) - \left[\int_0^{\pi/2} \frac{d^2 \Psi_d^T(c)}{dc^2} \sin^2 \theta \Big|_{c=a(t) \sin \theta} d\theta \right] \mathbf{x}_d(t) \right\} \dot{a}(t) \\ + \left[\int_0^{\pi/2} \frac{d\Psi_a^T(c)}{dc} \Big|_{c=a(t) \sin \theta} d\theta \right] \dot{\mathbf{x}}_a(t) - \left[\int_0^{\pi/2} \frac{d\Psi_d^T(c)}{dc} \Big|_{c=a(t) \sin \theta} \sin \theta d\theta \right] \dot{\mathbf{x}}_d(t). \quad (43b)$$

When $t = t_0 = 0$, i.e., when the wedge begins to dip into the water, the wetted length $a(t_0) = 0$. Physically, there is no hydrodynamic load acting on the wedge at this moment. Consequently, $\ddot{\mathbf{x}}_a$ and $\ddot{\mathbf{x}}_d$ can be obtained from Eq. (33) by disregarding the hydrodynamic loads. Then $\ddot{a}(t_0)$ is obtained from Eq. (42).

The numerical procedure is summarized as follows.

Step 1: Given initial conditions $a[t_0]$, $\mathbf{x}[t_0]$, find $\dot{a}[t_0]$ and $\ddot{a}[t_0]$ from Eqs. (34) and (42), respectively;

Step 2: for $k = 0$, calculate sequentially $a[t_1]$, $\mathbf{x}[t_1]$ and $\dot{a}[t_1]$;

Step 3: for $k = 1$, calculate sequentially $a[t_2]$, $\dot{a}[t_1]$, $\mathbf{x}[t_2]$, and $\dot{a}[t_2]$;

Step 4: for $k \geq 2$, calculate sequentially $a[t_{k+1}]$, $\dot{a}[t_k]$, $\mathbf{x}[t_{k+1}]$, and $\dot{a}[t_{k+1}]$;

Step 5: $k \leftarrow k + 1$, repeat step (4) until the slamming process ends or $a(t) \geq a_{max}$.

It is noted that $a[t_{k+1}]$ is obtained by applying the fourth-order Runge–Kutta method to Eq. (34), $\dot{a}[t_k]$ is obtained from Eq. (41), $\mathbf{x}[t_{k+1}]$ is derived from Eq. (C.2) given in Appendix C, and $\dot{a}[t_{k+1}]$ is obtained from Eq. (34). The truncation error for the fourth-order Runge–Kutta method is $\mathcal{O}(\Delta t^5)$, and it is $\mathcal{O}(\Delta t^2)$ for the central-difference method. For the recurrence relation (C.2), Δt is restricted by the numerical stability requirement and a prescribed truncation error ε_s [see e.g., Meirovitch (1997), pp. 212–213]

$$\left(\frac{\Delta t}{n_g}\right)^{n_t} \times \frac{[\mathfrak{N}(\mathcal{A}[t_k])]^{n_t}}{n_t} < \frac{\varepsilon_s}{n_g}, \quad \text{with } \varepsilon_s \ll 1. \quad (44)$$

Here, $\mathfrak{N}(\mathcal{A}[t_k])$ denotes the largest modulus of eigenvalues of matrix $\mathcal{A}[t_k]$, $(n_t + 1)$ is the number of terms used in the evaluation of the transition matrix $\exp(\mathcal{A}[t_k]\Delta t/n_g)$ in Eq. (C.2), and n_g is the number of subdivisions of Δt . Numerical calculations have shown that the hydroelastic effect has negligible influence on $\mathfrak{N}(\mathcal{A}[t_k])$ and it remains unchanged during the entire slamming process.

Due to the high stiffness to weight ratio of a typical sandwich panel, its natural frequencies are very high. This can cause ill conditioning of the system matrix \mathcal{A} in Eq. (33). This is overcome by using the dimensionless time variable $\omega_1 t$, with ω_1 being the fundamental frequency of the dry panel.

4. Verification of the algorithm

In order to verify the preceding numerical procedure, we simplify Eqs. (32) and (34) of the hydroelastic system in such a way that the added-mass, -damping and -stiffness terms in Eq. (32) and the structural deformation terms in Eq. (34) drop out. We further assume that the panel is a uniform straight single layer. Due to the availability of the analytical solution, we assume the beam to be simply supported at both ends. The small deadrise angle is denoted by β , and as a result, $z = f(y) = y \tan \beta$ describes the initial profile of the panel. In this case, governing Eqs. (23a)–(23d) and (18) reduce to

$$D_{22}^f \frac{\partial^4 w}{\partial y^4} + m_0^f \frac{\partial^2 w}{\partial t^2} = \frac{1}{2} p_s(y, t), \quad 0 < y < L, \quad (45)$$

where w denotes the deflection of the beam and p_s is the hydrodynamic pressure acting on the beam without considering its deformations. The initial conditions associated with Eq. (45) are taken as $w(y, 0) = \dot{w}(y, 0) = 0$, while the pertinent boundary conditions are $w(0) = w(L) = w''(0) = w''(L) = 0$ where $w' = \partial w / \partial y$.

We now find an expression for p_s . The Wagner condition (8) can be written as

$$a(t) = \frac{\pi}{2 \tan \beta} h(t), \quad (46)$$

and the distributed vortex intensity γ_b as

$$\gamma_b(\tilde{y}, t) = -\frac{4a^2(t) \tan \beta}{\pi} \tilde{y} \ln \left| \frac{1 + \sqrt{1 - \tilde{y}^2}}{\tilde{y}} \right|. \quad (47)$$

In dimensional (i.e., physical) variables, the displacement and the velocity potentials are given by

$$\Phi_h(y, 0^-, t) = \frac{1}{2} h(t) \sqrt{a^2(t) - y^2} - \frac{\tan \beta}{\pi} y^2 \ln \left| \frac{a(t) + \sqrt{a^2(t) - y^2}}{y} \right|, \quad (48a)$$

$$\frac{\partial \Phi_h(y, 0^-, t)}{\partial t} = \dot{h}(t) \sqrt{a^2(t) - y^2}. \quad (48b)$$

Eq. (46) is exactly the same as Eq. (9.17) in Faltinsen (1990) while Eq. (48b) is exactly the same as Eq. (2) in Mizoguchi and Tanizawa (1996). Substitution from Eq. (48a) into Eq. (11) gives the hydrodynamic pressure acting on beam's wetted surface (i.e., $0 < y < a(t) \leq L$) as

$$p_s(y, t) = \rho_h \left[\dot{h}(t) \sqrt{a^2(t) - y^2} + \frac{\pi \dot{h}^2(t)}{2 \tan \beta} \frac{a(t)}{\sqrt{a^2(t) - y^2}} \right], \quad (49)$$

and the corresponding total hydrodynamic load by

$$P_0(t) = \rho_h \left[\frac{\pi}{4} a^2(t) \dot{h}(t) + \frac{\pi^2 a(t) \dot{h}^2(t)}{4 \tan \beta} \right]. \tag{50}$$

For constant speed of penetration V , we have $h(t) = Vt$. Then, the solution of Eq. (45) can be represented as [see e.g., Meirovitch (1997), p. 387]:

$$w(y, t) = \sum_{k=1}^{\infty} W_k(y) c_k(t), \tag{51}$$

in which the generalized coordinate $c_k(t)$ is given by

$$c_k(t) = \frac{\rho_h \pi^3 V^3}{16 (\tan^2 \beta) \omega_{sk} M_{kk}} \int_0^t \sin[\omega_{sk}(t - \tau)] \tau \mathcal{H}_0 \left[\frac{k\pi}{L} a(\tau) \right] d\tau. \tag{52}$$

Here, $\mathcal{H}_0[\cdot]$ denotes the Struve function of order 0, while ω_{sk} and M_{kk} are defined as

$$\omega_{sk} = \frac{k^2 \pi^2}{L^2} \sqrt{\frac{D_{22}^f}{m_0^f}}, \quad M_{kk} = \frac{L}{2} m_0^f, \quad k = 1, 2, \dots. \tag{53}$$

For values of various variables listed in the figure caption, Fig. 3 shows time histories of evolution of c_1 , c_2 and c_3 . It is clear that for $t \geq 4$ ms, $|c_2|$ and $|c_3|$ are considerably smaller than $|c_1|$. In fact, $|c_2|$ and $|c_3|$ are essentially zero. Thus even one mode in Eq. (51) gives a fairly accurate solution. Similar results on including a small number of terms in Eq. (51) have been reported in the literature (see e.g., Faltinsen, 1999).

For values of different parameters listed in the caption of Fig. 4, we compare the analytical solution of the problem with its numerical solutions computed by taking $\Delta t = 1/(5\omega_0)$ and $\Delta t = 1/(20\omega_0)$ where ω_0 is the fundamental natural frequency of the simply supported beam. It is evident that the two time steps give very close results, and the numerical solution agrees well with the analytical solution of the problem.

5. Results and discussion

The {3,2}-order sandwich panel theory used here is based on a general 3D curved sandwich shell theory proposed by Hohe and Librescu (2003). For validating the structural model developed in the present paper and the numerical approach based on EGM, we calculate natural frequencies of a dry sandwich panel and compare them in Table 1 with those obtained by using the commercial code ABAQUS®. Both the top and the bottom face sheets are made of an orthotropic material, while the core is made of an isotropic material. Values of material and geometric parameters of the panel are: $E_{22}^f = 138$ GPa, $E_{33}^f = 8.96$ GPa, $\nu_{23}^f = 0.3$, $G_{23}^f = 7.1$ GPa, $E^c = 2.8$ GPa, $\nu^c = 0.3$, $\rho^f = 31,400$ Kg/m³, $\rho^c = 150$ Kg/m³,

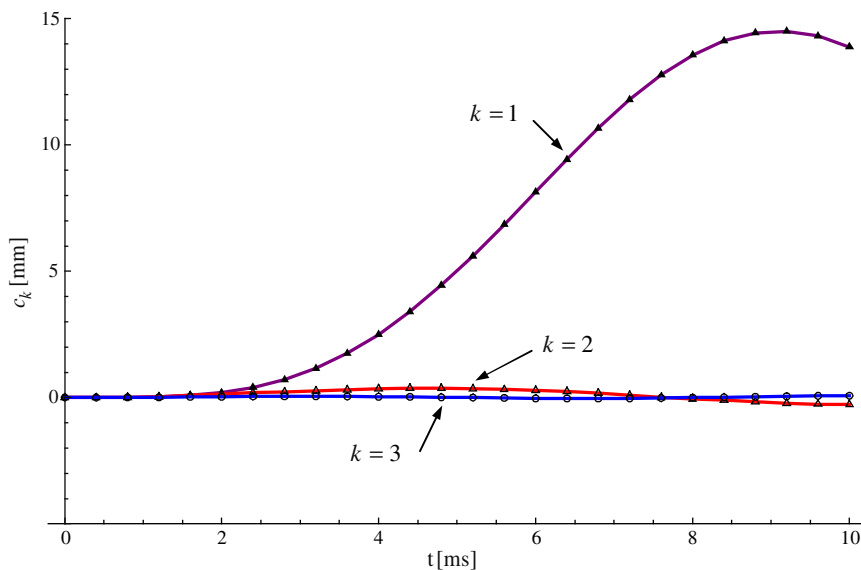


Fig. 3. Variation with time of the generalized coordinate c_k in Eq. (52) associated with the first three eigenmodes. $D_{22}^f = 7.29 \times 10^5$ Nm, $m_0^f = 135$ Kg/m², $V = 10$ m/s, $\beta = 10^\circ$, $L = 1.0$ m.

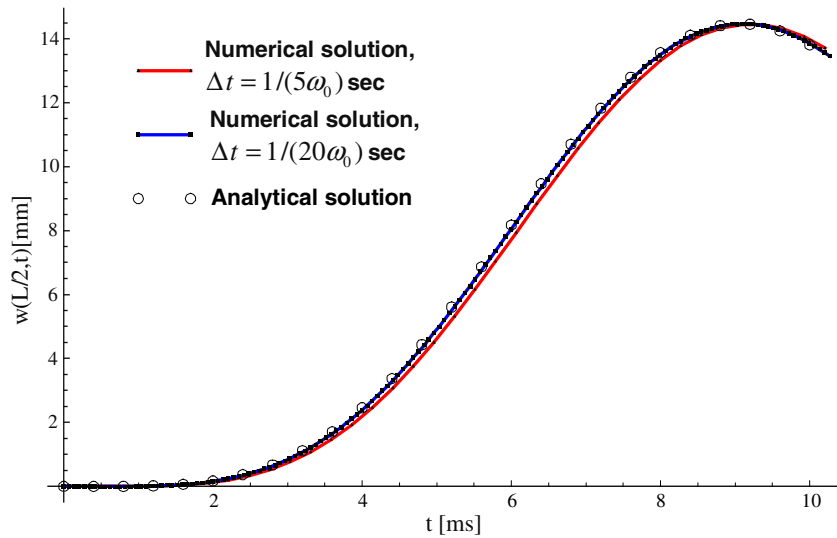


Fig. 4. Comparison of the analytical solution with the numerically computed time histories of the mid-span deflection with two different values of the time step. The associated parameters are: $D_{22}^f = 7.29 \times 10^5$ Nm, $m_0^f = 135$ Kg/m², $V = 10$ m/s, $\beta = 10^\circ$, $L = 1.0$ m, $\omega_0 = 725.4$ rad/s.

Table 1
Convergence of the first four frequencies with increase in the number of basis functions

N_s	kth natural frequency (rad/s)			
	$k = 1$	$k = 2$	$k = 3$	$k = 4$
2	738.0(5.0% ^a)	1922.2(25.3%)	–	–
3	731.2(4.0%)	1631.5(6.38%)	2921.4(16.3%)	–
4	725.7(3.2%)	1614.4(5.2%)	2670.1(6.3%)	3991.8(12.4%)
5	721.9(2.7%)	1604.9(4.6%)	2649.2(5.4%)	3779.9(6.4%)
6	721.1(2.6%)	1595.4(4.0%)	2639.4(5.1%)	3759.0(5.8%)
7	719.2(2.3%)	1593.6(3.9%)	2627.7(4.6%)	3750.2(5.6%)
8	719.0(2.3%)	1588.8(3.5%)	2625.7(4.5%)	3738.5(5.2%)
By ABAQUS [®]	703.1	1534.4	2512.3	3552.3

^a Relative error, $([\text{prediction by the present model}] - [\text{result by ABAQUS}^{\text{®}}]) / [\text{result by ABAQUS}^{\text{®}}] \times 100\%$.

$t^f = 12$ mm, $t^c = 30$ mm, $L = 1.0$ m. In using ABAQUS[®], the quadratic plane-strain element CPE8R is used for both the core and the face sheets. Ends of the face sheets are taken to be clamped, whereas those of the core are taken as hinged. The discretization of the panel into finite elements is shown in Fig. 5. Nodes of the core and the face sheets at their common interfaces are tied to ensure continuity of displacements.

It is seen from Table 1 that natural frequencies predicted by the present {3,2}-order theory are close to those computed with ABAQUS[®], and the convergence is fast. Table 2 lists the corresponding prediction of the mode shapes. Recalling that even one term in Eq. (51) gives an accurate solution for transient deformations of the simply supported beam, we henceforth take $N_s = 3$ in Eqs. (26a) and (26b). Besides $a(t)$, the number of unknowns in Eqs. (32) and (33) are 12 and 24, respectively. Polynomials of degree 16 in y approximate the first three shape functions in Eq. (27) with the variance less than 3×10^{-20} , and expressions of these polynomials are given in Eqs. (B.7,8).

For results given in Figs. 6–14, the material properties of the face sheets and the core are the same as those used above to compute frequencies. In order to consider the nonstructural mass associated with the hull and to avoid bow flare slamming, the mass density of the material of the face sheets is taken as $\rho^f = 31,400$ Kg/m³. Unless otherwise stated, the deadrise angle β is taken as 5° . Other parameters used in calculations are: $\omega_1 = 731.2$ rad/s, $\Delta t \omega_1 = 0.1$, $n_g = 10$, $n_t = 30$, $\epsilon_s \leq 10^{-6}$.

In the present problem, the hydroelastic effect manifests itself in two places: (1) the added-mass, -damping and -stiffness in Eq. (32); (2) the contact point $a(t)$ whose position is influenced by structural deformations, as shown by Eqs. (34) and



Fig. 5. Finite element mesh used for the analysis with ABAQUS/Standard.

Table 2

Comparison of the first four modes shapes computed with the present {3,2}-order sandwich theory and with the commercial code ABAQUS®

Mode Shape #	Mode shape predicted by the present model ($N_s = 8$).	By ABAQUS
1		
2		
3		
4		

These four modes correspond to flexural deformations in which the averaged deflection u_3^a is dominant, and the other three displacement components have negligible values as compared to that of u_3^a and are omitted from mode shapes depicted in the second column.

(35a), (35b). The evaluation of the added-mass, -damping and -stiffness takes more CPU time than that for evaluating $a(t)$. To facilitate efficient evaluation of the hydroelastic effect on the slamming response, we consider individual contributions from each of these two manifestations. The model which accounts for both effects is termed below as Model I, while the one accounting for only the second part is called Model II. When neither effect is incorporated, the model is referred to as Model III. We note that in model III, the pressure distribution on the deformable wedge equals that on the rigid wedge. Fig. 6 shows time histories of the mid-span deflection computed with the three models. It is clear that the hydroelastic effect noticeably

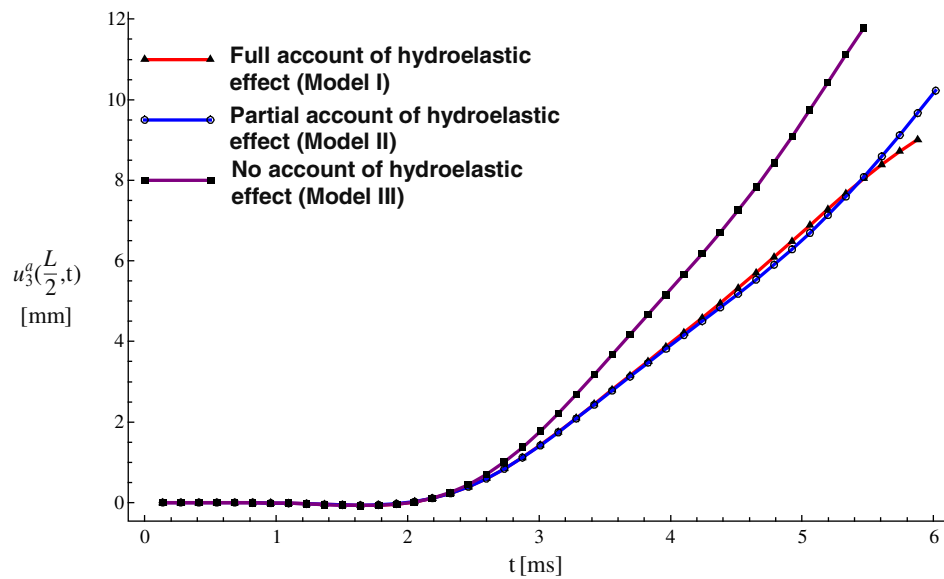


Fig. 6. Time history of the mid-span deflection during the slamming impact ($V = 10$ m/s).

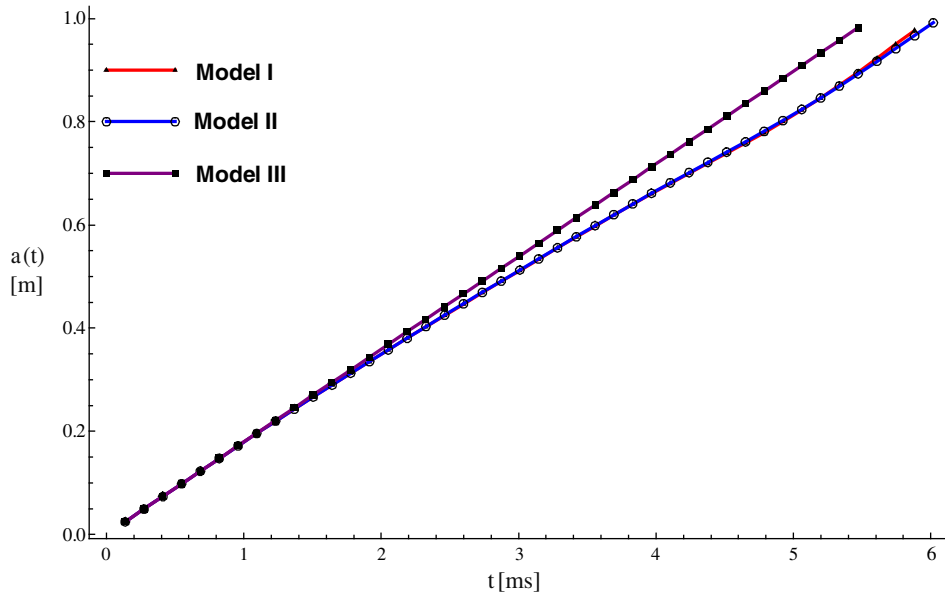


Fig. 7. Time history of the length $a(t)$ of the wetted surface ($V = 10$ m/s).

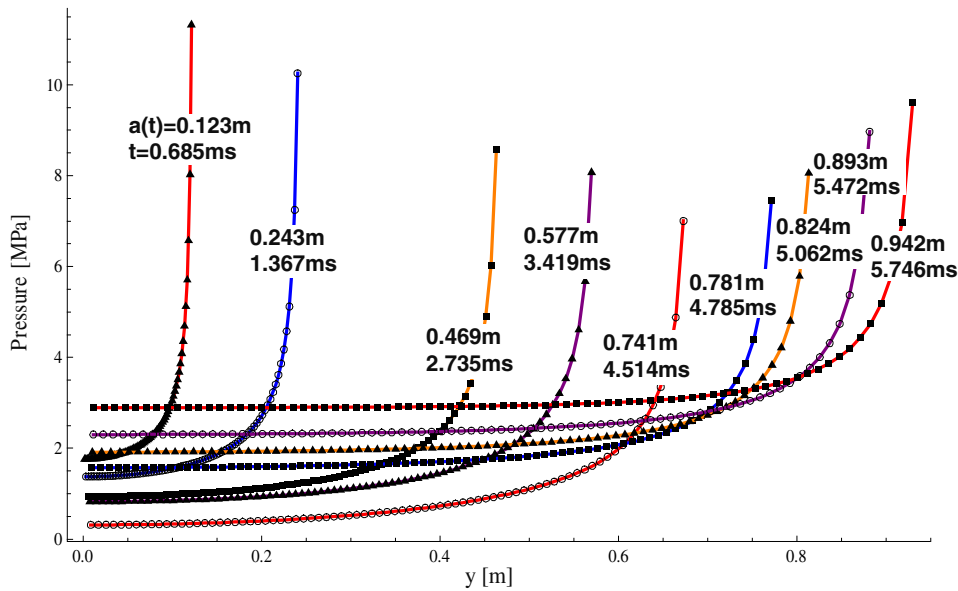


Fig. 8. Distribution of the hydrodynamic pressure along the slammed wedge ($V = 10$ m/s). Results are computed with Model II.

decreases the deflection of the slammed wedge, and as the slamming impact progresses, this decrease becomes more significant. Furthermore, as far as the deflection response is concerned, Model II captures nearly all of the hydroelastic effect.

Fig. 7 depicts the time history of length $a(t)$ of the wetted surface computed with the three models. It is seen that neglecting of the hydroelastic effect results in earlier wetting of the entire length of the wedge. Once again, results computed with Model II agree very well with those obtained from Model I. Henceforth, we use Model II to compute results.

Fig. 8 displays, for different wetted lengths, the hydrodynamic pressure distributed along the wetted part of the wedge. Each curve corresponds to a different stage of the slamming process, as marked by the values of $a(t)$ and the corresponding times. According to the Wagner theory of water impact developed in Section 3, there is a reciprocal square root singularity at the end of the wetted wedge, see e.g., Eq. (49) for a rigid straight wedge. The order of singularity remains the same for a deformable wedge. For results presented in Fig. 8, the numerical evaluation of the pressure was terminated at $y = 0.9875a(t)$. Note that the pressure at a point within the wetted wedge varies with time t during slamming.

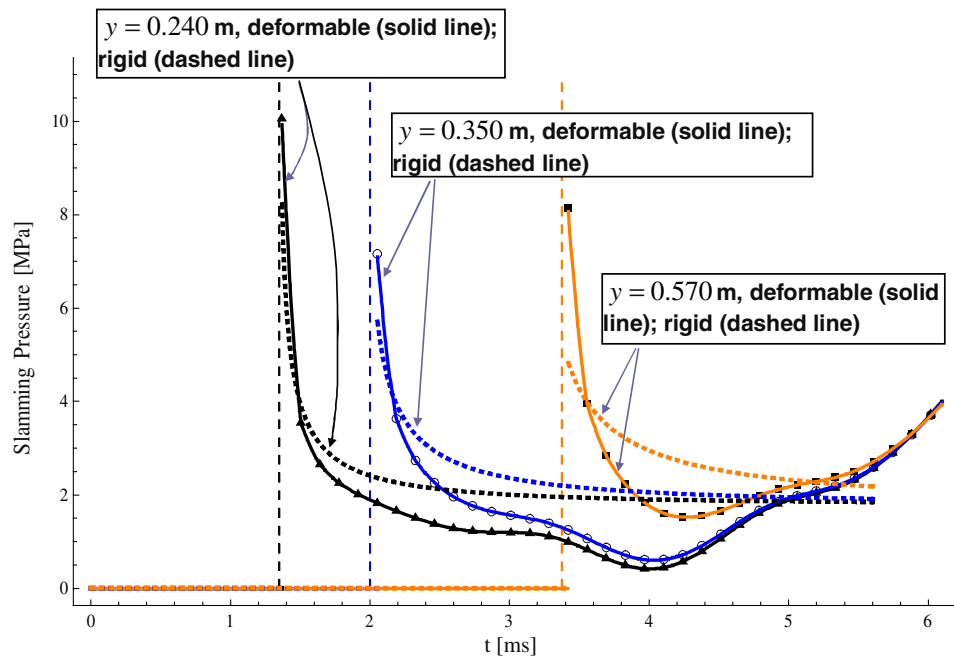


Fig. 9. Time history of the slamming pressure at three locations on the wedge: $y = 0.240$, 0.350 and 0.570 m. The three vertical dashed lines at $t = 1.349$, 2.004 and 3.374 ms denote the time when water reaches these locations. Due to singularity at the end of wetted wedge, the times to record the pressure start at $t = 1.367$, 2.052 and 3.419 ms, respectively.

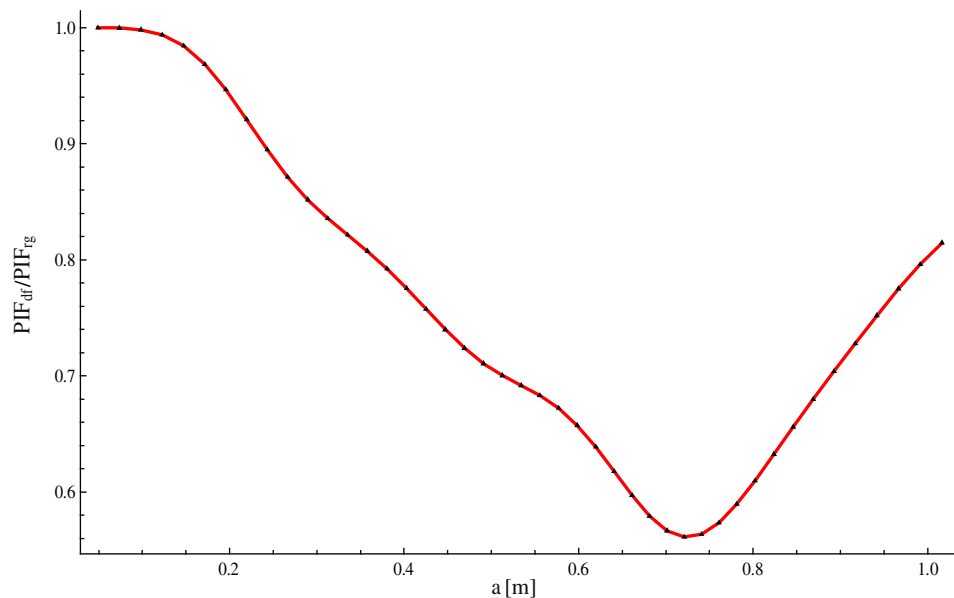


Fig. 10. Ratio of the pressure intensity factor of the (deformable) wedge (PIF_{df}) to the pressure intensity factor of the corresponding rigid wedge (PIF_{rg}) versus the wetted length $a(t)$. Results are computed with Model II.

At three locations of the wedge during the slamming process, Fig. 9 shows the hydrodynamic pressure versus time. For comparison, results for a rigid wedge computed from Eq. (49) are also included. Notice the merge of the three pressures for the deformable wedge at the terminal stage of the slamming process. This agrees with the results plotted in Fig. 8 where the hydrodynamic pressure along most of the wedge length is uniform at the terminal stage of the slamming.

For a rigid wedge, from Eqs. (46) and (49), we get

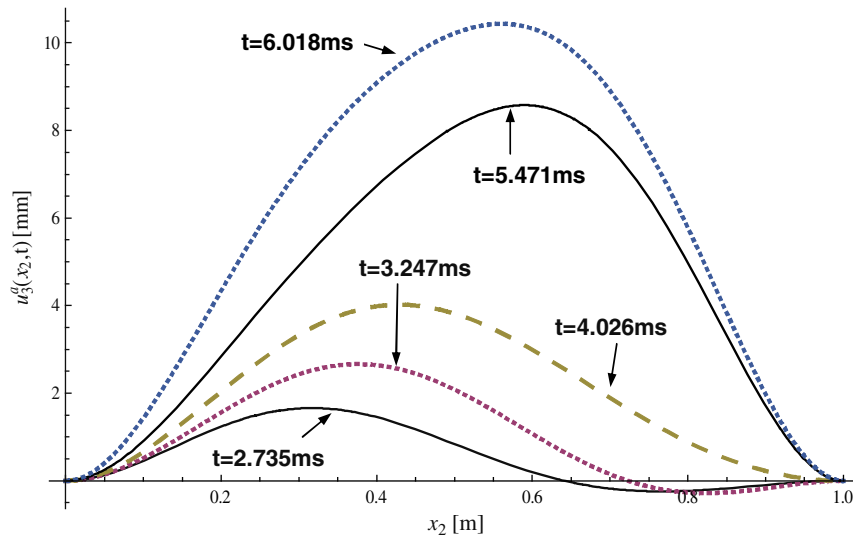


Fig. 11. Deflected shape of the panel at five slamming stages ($V = 10$ m/s). Results are computed with Model II.

$$PIF_{rg}(t) = \left(\frac{\pi}{2 \tan \beta} \right)^2 \rho_h V^3 t, \tag{54}$$

Fig. 10 shows the ratio of the pressure intensity factor of the (deformable) wedge, $PIF_{df}(t)$, over $PIF_{rg}(t)$. We see that deformations of the wedge significantly reduce the peak pressure intensity over the entire slamming process, and the maximum reduction of 44% occurs when the wetted length $a(t) = 0.73$ m.

Fig. 11 depicts the lengthwise distribution of the average displacement $u_3^a(x_2, t)$ of the two face sheets' mid-surfaces at five selected impact stages corresponding to $t = 2.735, 3.247, 4.026, 5.471$ and 6.018 ms. It is interesting to notice that the location of the peak value of $u_3^a(x_2, t)$ shifts with time t , but not monotonically to one direction. In Fig. 12, the deformed shapes of the entire panel at $t = 2.735$ and 6.018 ms are displayed. We note that the peak deflection at the terminal stage of the slamming occurs at $x_2 \approx 0.57$ m.

Fig. 13a and b exhibit distributions of the strain energy density stored in the two face sheets and the core at an early and at a terminal stage of the slamming impact, respectively. The strain energy density at a point in the panel can be represented as

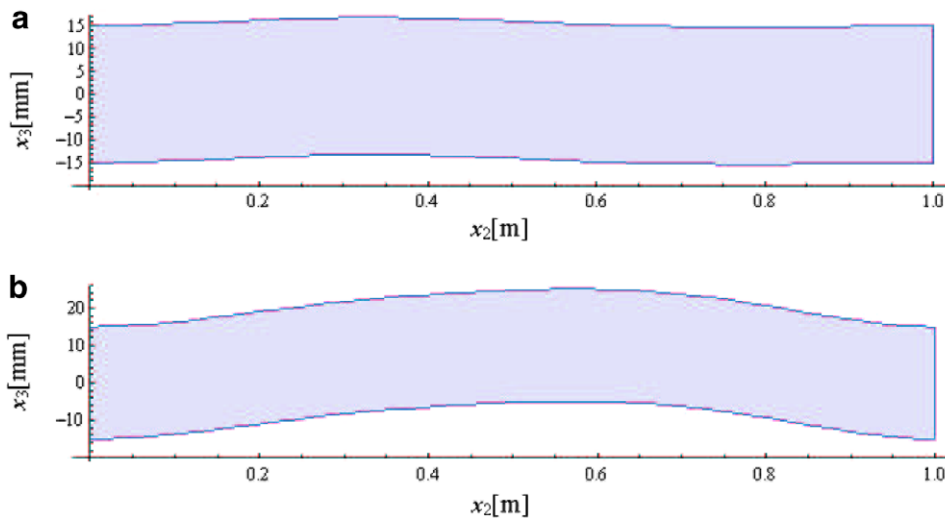


Fig. 12. Deformed shapes of the panel at (a) an early stage of slamming $t = 2.735$ ms, and (b) an ending stage $t = 6.018$ ms. ($V = 10$ m/s). Results are computed with Model II.

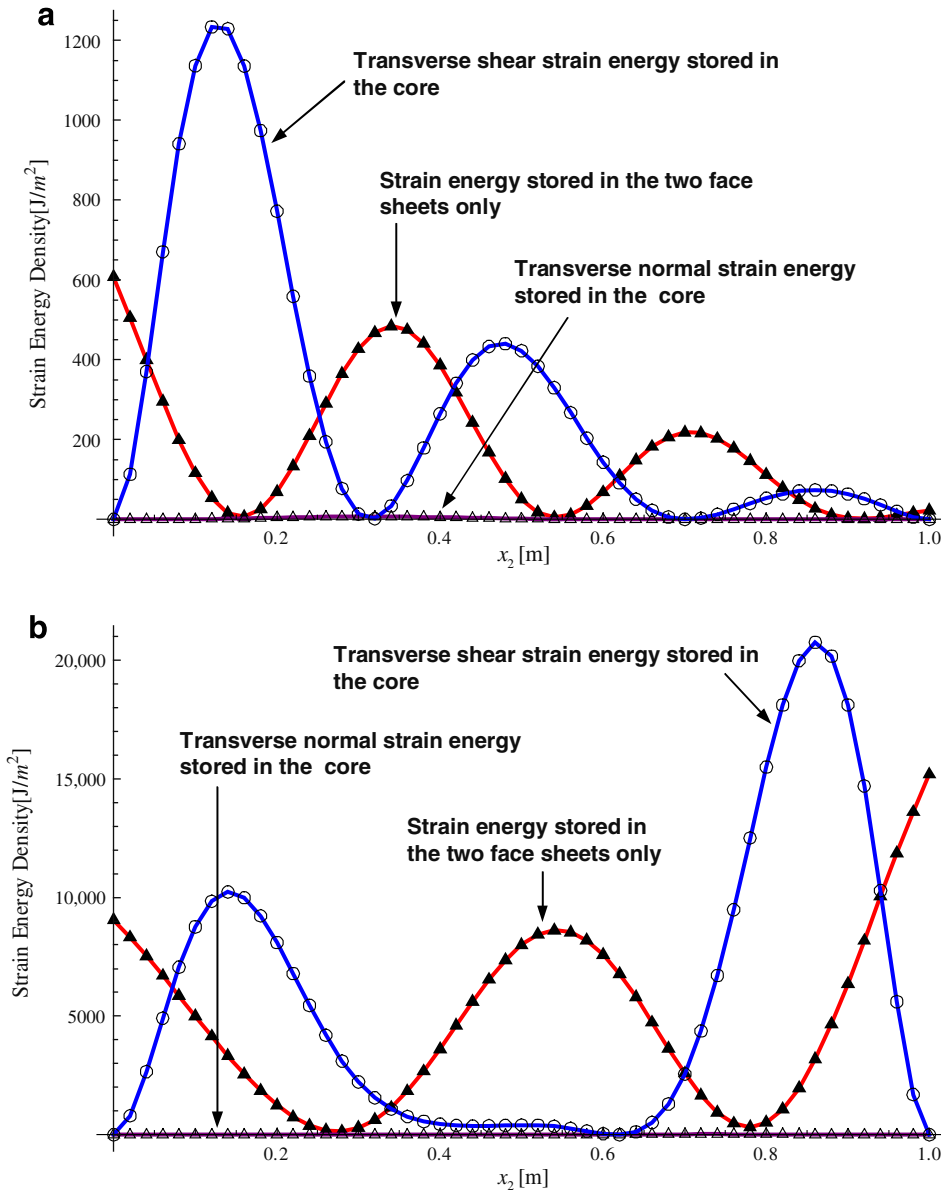


Fig. 13. Strain energy density in the core and face sheets at (a) an early stage of slamming $t = 2.735$ ms; (b) an ending stage $t = 6.018$ ms ($V = 10$ m/s). Results are computed with Model II.

$$U = \underline{A_{22}^f (u_{2,2}^d)^2} + \underline{D_{22}^f (u_{3,22}^a)^2} + \underline{D_{22}^f (u_{3,22}^d)^2} + \underline{\frac{2A_{33}^c}{(t^c)^2} (u_3^d)^2} + \underline{\frac{32D_{33}^c}{(t^c)^2} (\Phi_3^c)^2} + \underline{\frac{1}{2} A_{23}^c \left[\frac{2}{t^c} u_2^d + \left(1 + \frac{t^f}{t^c}\right) u_{3,2}^a - \frac{2}{3} \Phi_{3,2}^c \right]^2} \quad (55)$$

Here, terms underlined by the single solid straight line denote the strain energy density at a point of the face sheets, terms underscored by the double solid line equal the strain energy density at a point in the core associated with the transverse normal strain, and terms underscored by the wavy line denote the strain energy density at a point in the core associated with the transverse shear strain. From results shown in Fig. 13a and b, it is readily seen that (1) the core absorbs considerable portion of the energy of deformation; (2) the strain energy in the core is dominantly contributed by the transverse shear strain; (3) the portion of the strain energy due to the transverse normal strain in the core is negligibly small; (4) locations of the wedge where the strain energy density in the core is large have small values of the strain energy density in the core, and vice versa. This implies that the core can be effectively used to absorb a major

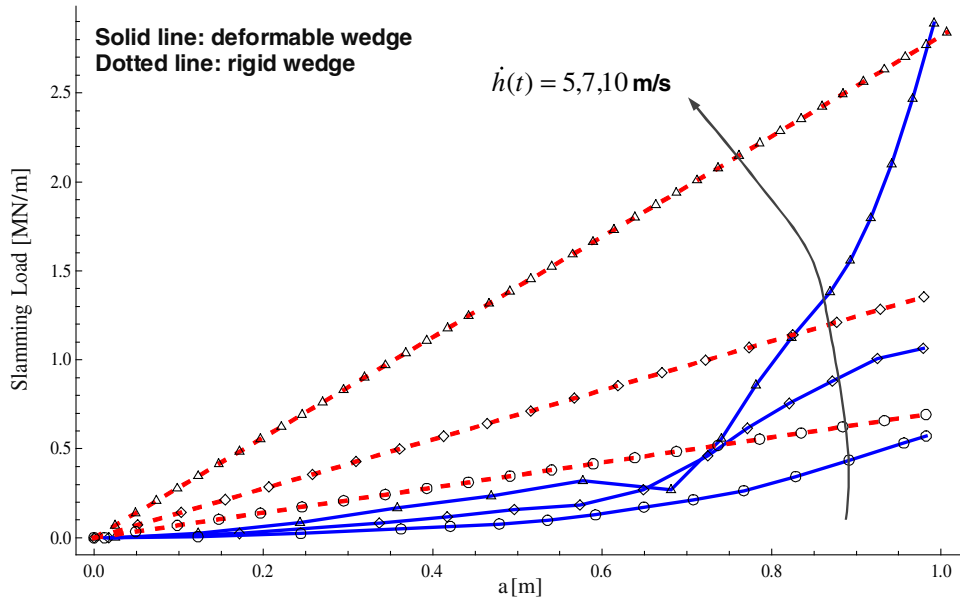


Fig. 14. Total slamming load P_0 versus $a(t)$ for three penetration speeds. Results are computed with Model II.

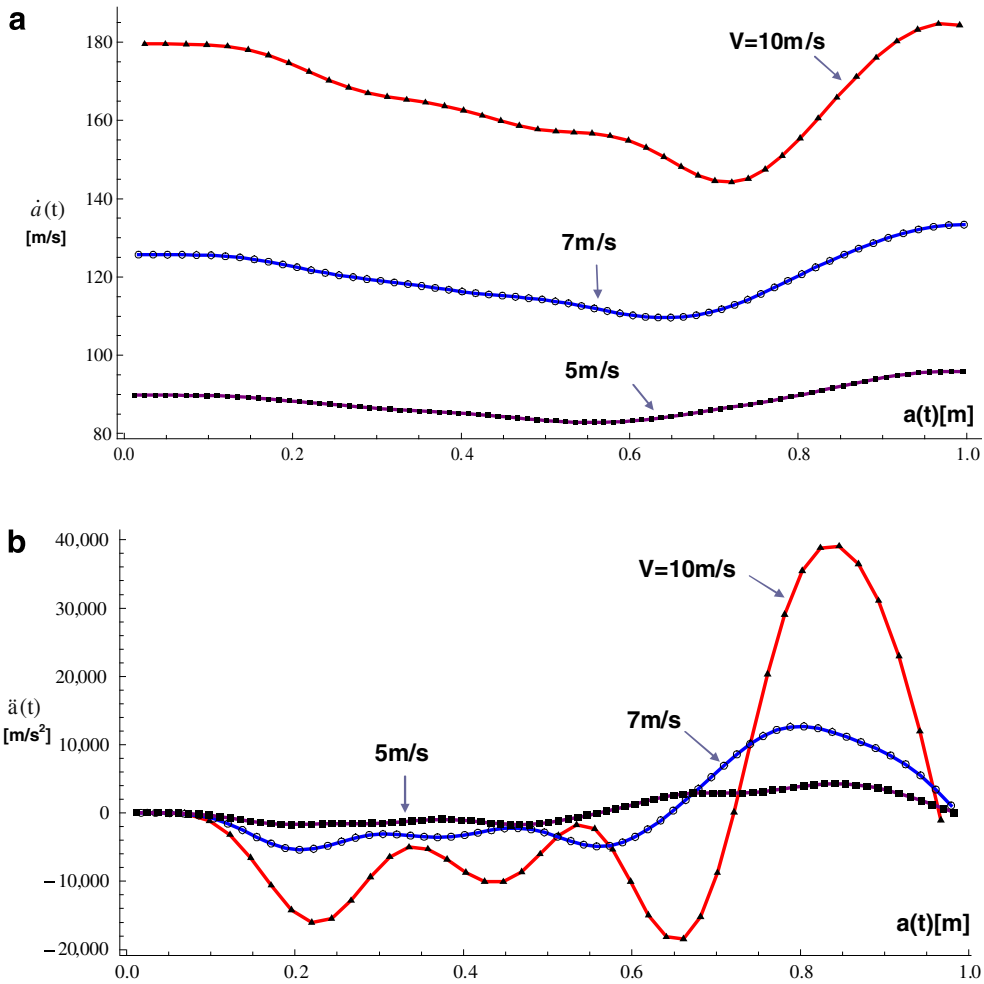


Fig. 15. (a) $\dot{a}(t)$ versus $a(t)$ for three penetration speeds; (b) $\ddot{a}(t)$ versus $a(t)$ for three penetration speeds. Results are computed with Model II.

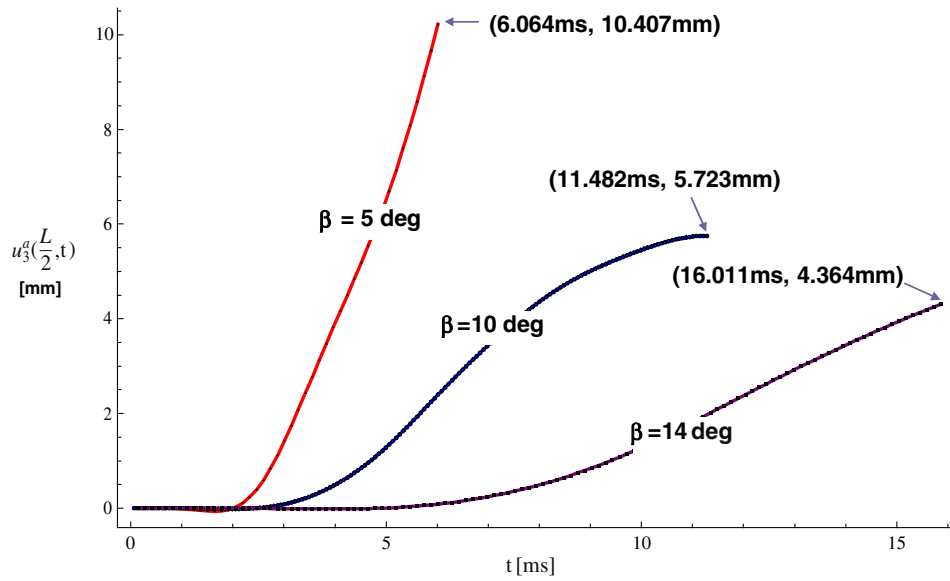


Fig. 16. Time histories of the mid-span deflection of the wedge for three deadrise angles: $\beta = 5^\circ, 10^\circ, 14^\circ$. For each case, the time for water to wet the entire wedge and the amplitude of the mid-span deflection at the last moment of slamming process are shown in parentheses. The results are computed with Model II.

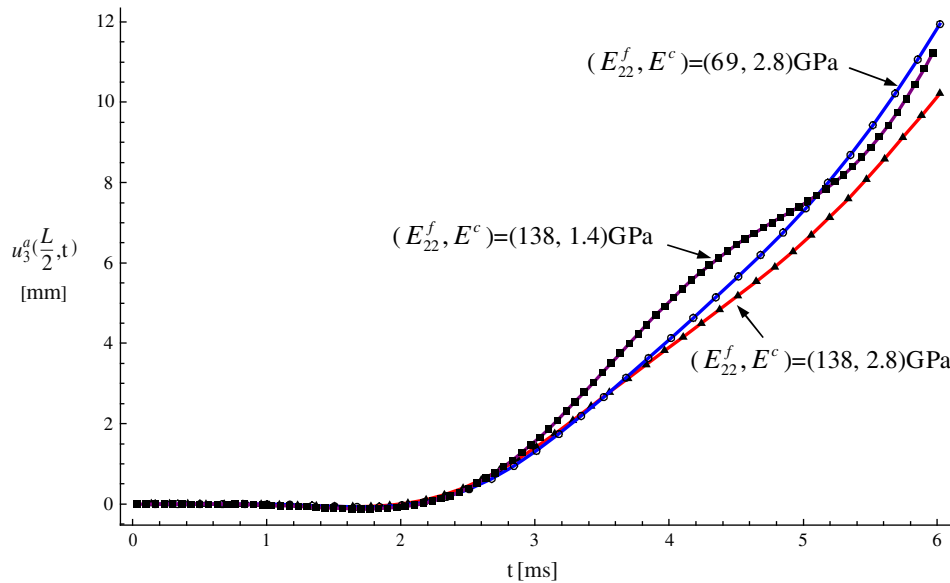


Fig. 17. Influence of the weakening of E_{22}^f and E^c on deflection of the wedge at $y = L/2$ ($V = 10$ m/s). The results are computed with Model II.

part of the slamming impact energy. As should be evident from the scales on the vertical axes in Fig. 13a and b, the strain energy density at the terminal stage $t = 6.018$ ms of the slamming is nearly 15 times that at $t = 2.735$ ms. Of course, deformations of the sandwich structure depend upon boundary conditions, and results presented herein are applicable only when the two edge surfaces are clamped.

For penetration speeds of 5, 7 and 10 m/s, Fig. 14 shows the total slamming load $P_0(t)$ versus the wetted length $a(t)$. Recalling that $P_0(t)$ is defined by Eq. (39), the total slamming load for a given value of $a(t)$ equals area under the curve of Fig. 8. We note that (1) during most of the slamming process, the total slamming load on the deformable wedge is considerably smaller than that on the rigid wedge, and with the increase of the penetration speed, the difference between the two loads increases; (2) in the second half stage of the slamming process, the hydroelastic effect induces a more rapid increase of the slamming load on the

deformable wedge than the increase observed on the rigid wedge. As evidenced by the slope of the curves, the rate of increase of the total slamming load with respect to the wetted length during the second half of the impact process is intensified with an increase in the penetration speed. Results plotted in Fig. 14 suggest that the consideration of loads acting on a rigid wedge will give a conservative design of the wedge unless deformations also depend upon the loading rate.

For $V = 10$ m/s, the total slamming load decreases from $a(t) = 0.57$ to $a(t) = 0.67$ m, and subsequently increases monotonically. For $V = 5$ and 7 m/s, the total slamming load increases monotonically during the entire slamming process.

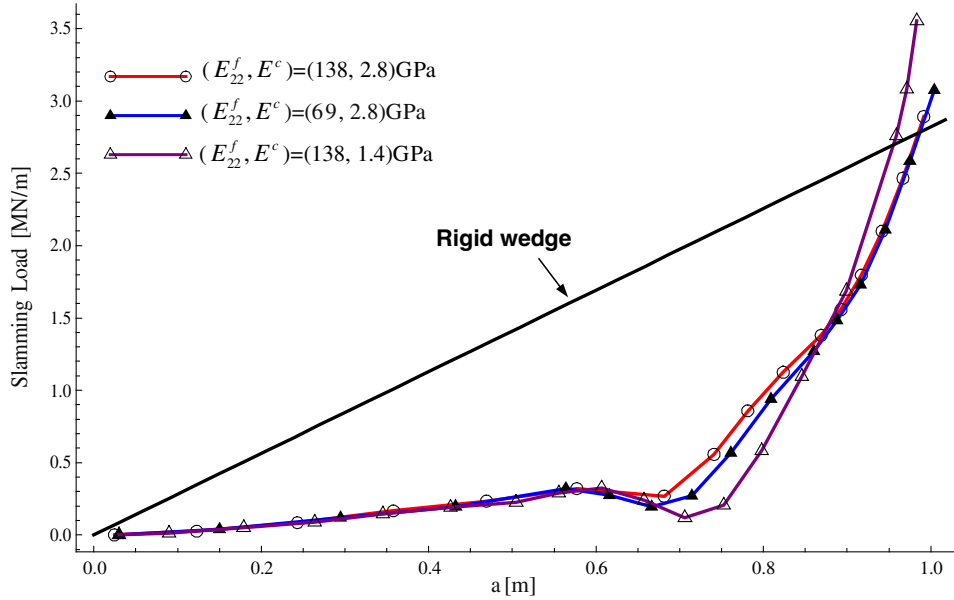


Fig. 18. Influence of the weakening of E_{22}^f or E^c on the total slamming load ($V = 10$ m/s). The results are computed with Model II.

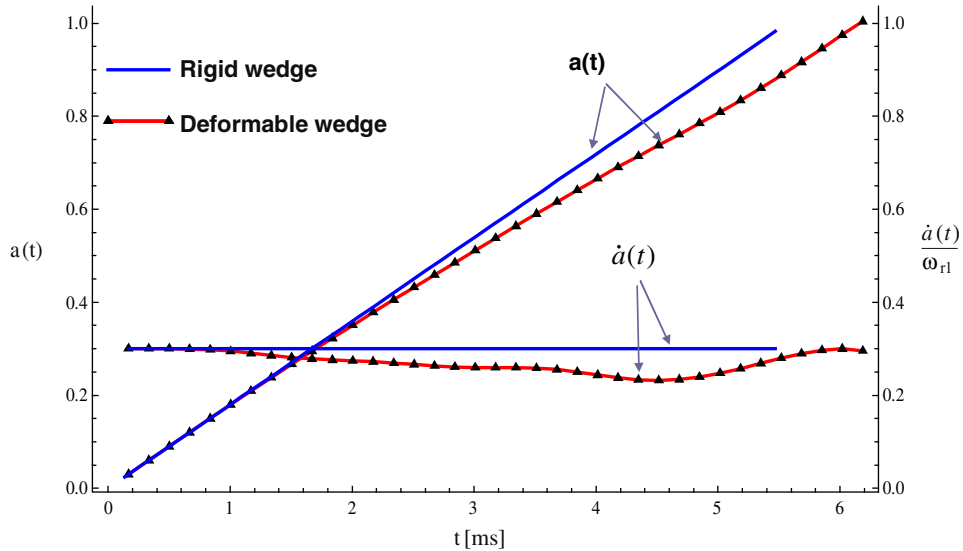


Fig. 19. Time history of $a(t)$ and $\dot{a}(t)$ for the rigid wedge and the face sheets- weakened wedge $(E_{22}^f, E^c) = (69, 2.8)$ GPa during the slamming process. $\omega_{r1} = 598.0$ rad/s. The results are computed with Model II.

Fig. 15 delineates the influence of the penetration speed on $\dot{a}(t)$ and $\ddot{a}(t)$. The decrease of $\dot{a}(t)$ at the beginning of the slamming process and the oscillations in $\ddot{a}(t)$ are due to the hydroelastic effect. We observe that with the increase of V from 5 to 10 m/s, the location where $\dot{a}(t)$ reaches minimum shifts to the right end of the wedge in Fig. 15a while $\ddot{a}(t)$ plotted in Fig. 15b becomes more oscillatory and its peak amplitude increases dramatically.

Fig. 16 shows the time histories of the mid-span deflection of the wedge for three deadrise angles $\beta = 5^\circ, 10^\circ$ and 14° . We note that as β increases from 5° to 10° (14°), the time taken to wet the entire wedge increases by 90% (170%), while the mid-span deflection at the end of the slamming process decreases by 45% (58%).

Figs. 17 and 18 show, respectively, time histories of the deflection at the mid-span $y = L/2$ and the variation with the wetted length of the total slamming load on the panel when either the elastic modulus E_{22}^f of the face sheets or E^c of the core is reduced by a factor of two. Other parameters are: $n_g = 10$, $n_t = 30$. For $(E_{22}^f, E^c) = (138, 1.4)$ GPa, $\omega_1 = 599.9$ rad/s, $\Delta t\omega_1 = 0.02$; and for $(E_{22}^f, E^c) = (69, 2.8)$ GPa, $\omega_1 = 598.0$ rad/s, $\Delta t\omega_1 = 0.1$. It is clearly observed from the results depicted in Figs. 17 and 18 that the weakening of the core noticeably intensifies the rate of increase of the slamming load with respect to the wetted length during the second half of the impact process, while decreasing the axial modulus E_{22}^f of the face sheets has a marginal influence on the slamming load. It is also seen from Fig. 18 that the largest dip in the slamming load occurs for $(E_{22}^f, E^c) = (138, 1.4)$ GPa.

Fig. 19 displays the time history of the wetted length $a(t)$ and of $\dot{a}(t)$ during the entire slamming process of the weakened wedge with $(E_{22}^f, E^c) = (69, 2.8)$ GPa. It is clear that during most of the slamming process, deformations of the wedge decrease $\dot{a}(t)$.

6. Conclusions

A comprehensive model to study the fluid–structure interaction during hull's slamming entry into calm water has been developed. It predicts the slamming load and the response of the sandwich composite hull. The slammed area of the hull is idealized as a deformable sandwich wedge. The structural part of the model incorporates core's transverse flexibility and has been validated by comparing natural frequencies of a dry sandwich panel with those computed by using the commercial finite element code ABAQUS®. Wagner's water impact theory is extended to account for deformations of the structure. The governing equations are nonlinear because the a priori unknown wetted area depends upon deformations of the structure which themselves are to be found. A numerical solution procedure has been developed to solve the coupled nonlinear governing equations. The numerical algorithm has been verified by comparing results for a simple problem with those from its analytical solution. Major conclusions are:

- the hydroelastic effect has a noticeable influence on the deflection response, and it significantly changes the hydrodynamic load,
- the core absorbs a considerable part of the strain energy due to its transverse shear deformations, which implies that the core can be effectively used for slamming impact alleviation,
- major influence of the hydroelastic effect can be effectively captured by Model II, which disregards the time-consuming evaluation of added-mass, -damping and -stiffness matrices and only considers the influence of structural deformations on the wetted length $a(t)$, and the hydrodynamic pressure.

Acknowledgments

The financial support of the Office of Naval Research, Solid Mechanics Program, Grants N00014-06-1-0913 and N00014-06-1-0567 to Virginia Polytechnic Institute and State University, and the interest and encouragement of the Program Manager, Dr. Y.D.S. Rajapakse, are gratefully acknowledged. The authors are indebted to Dr. Davresh Hasanyan for bringing to their attention the use of Hilbert transforms to analytically evaluate some singular integrals, and to Engineering Mechanics doctoral students S.S. Gupta and G. Gopinath for their help in using the commercial code ABAQUS®. Views expressed in this paper are those of the authors, and neither of the Program Manager nor other persons acknowledged herein, nor of the funding agency nor of their institutions.

Appendix A. Expressions for I_k ($k = 0, 16$)

$$I_0(\bar{y}) = 0,$$

$$I_1(\bar{y}) = \frac{2\bar{y}}{\sqrt{1-\bar{y}^2}} \ln \left| \frac{1 + \sqrt{1-\bar{y}^2}}{\bar{y}} \right|,$$

$$I_2(\tilde{y}) = \pi\tilde{y},$$

$$I_3(\tilde{y}) = 2\tilde{y} + \frac{2\tilde{y}^3}{\sqrt{1-\tilde{y}^2}} \ln \left| \frac{1 + \sqrt{1-\tilde{y}^2}}{\tilde{y}} \right|,$$

$$I_4(\tilde{y}) = \pi\tilde{y}^3 + \frac{\pi}{2}\tilde{y},$$

$$I_5(\tilde{y}) = \frac{2\tilde{y}^5}{\sqrt{1-\tilde{y}^2}} \ln \left| \frac{1 + \sqrt{1-\tilde{y}^2}}{\tilde{y}} \right| + 2\tilde{y}^3 + \frac{4}{3}\tilde{y},$$

$$I_6(\tilde{y}) = \pi\tilde{y}^5 + \frac{\pi}{2}\tilde{y}^3 + \frac{3\pi}{8}\tilde{y},$$

$$I_7(\tilde{y}) = \frac{2\tilde{y}^7}{\sqrt{1-\tilde{y}^2}} \ln \left| \frac{1 + \sqrt{1-\tilde{y}^2}}{\tilde{y}} \right| + 2\tilde{y}^5 + \frac{4}{3}\tilde{y}^3 + \frac{16}{15}\tilde{y},$$

$$I_8(\tilde{y}) = \pi\tilde{y}^7 + \frac{\pi}{2}\tilde{y}^5 + \frac{3\pi}{8}\tilde{y}^3 + \frac{5\pi}{16}\tilde{y},$$

$$I_9(\tilde{y}) = \frac{2\tilde{y}^9}{\sqrt{1-\tilde{y}^2}} \ln \left| \frac{1 + \sqrt{1-\tilde{y}^2}}{\tilde{y}} \right| + 2\tilde{y}^7 + \frac{4}{3}\tilde{y}^5 + \frac{16}{15}\tilde{y}^3 + \frac{32}{35}\tilde{y},$$

$$I_{10}(\tilde{y}) = \pi\tilde{y}^9 + \frac{\pi}{2}\tilde{y}^7 + \frac{3\pi}{8}\tilde{y}^5 + \frac{5\pi}{16}\tilde{y}^3 + \frac{35\pi}{128}\tilde{y},$$

$$I_{11}(\tilde{y}) = \frac{2\tilde{y}^{11}}{\sqrt{1-\tilde{y}^2}} \ln \left| \frac{1 + \sqrt{1-\tilde{y}^2}}{\tilde{y}} \right| + 2\tilde{y}^9 + \frac{4}{3}\tilde{y}^7 + \frac{16}{15}\tilde{y}^5 + \frac{32}{35}\tilde{y}^3 + \frac{256}{315}\tilde{y},$$

$$I_{12}(\tilde{y}) = \pi\tilde{y}^{11} + \frac{\pi}{2}\tilde{y}^9 + \frac{3\pi}{8}\tilde{y}^7 + \frac{5\pi}{16}\tilde{y}^5 + \frac{35\pi}{128}\tilde{y}^3 + \frac{63\pi}{256}\tilde{y},$$

$$I_{13}(\tilde{y}) = \frac{2\tilde{y}^{13}}{\sqrt{1-\tilde{y}^2}} \ln \left| \frac{1 + \sqrt{1-\tilde{y}^2}}{\tilde{y}} \right| + 2\tilde{y}^{11} + \frac{4}{3}\tilde{y}^9 + \frac{16}{15}\tilde{y}^7 + \frac{32}{35}\tilde{y}^5 + \frac{256}{315}\tilde{y}^3 + \frac{512}{693}\tilde{y},$$

$$I_{14}(\tilde{y}) = \pi\tilde{y}^{13} + \frac{\pi}{2}\tilde{y}^{11} + \frac{3\pi}{8}\tilde{y}^9 + \frac{5\pi}{16}\tilde{y}^7 + \frac{35\pi}{128}\tilde{y}^5 + \frac{63\pi}{256}\tilde{y}^3 + \frac{231\pi}{1024}\tilde{y},$$

$$I_{15}(\tilde{y}) = \frac{2\tilde{y}^{15}}{\sqrt{1-\tilde{y}^2}} \ln \left| \frac{1 + \sqrt{1-\tilde{y}^2}}{\tilde{y}} \right| + 2\tilde{y}^{13} + \frac{4}{3}\tilde{y}^{11} + \frac{16}{15}\tilde{y}^9 + \frac{32}{35}\tilde{y}^7 + \frac{256}{315}\tilde{y}^5 + \frac{512}{693}\tilde{y}^3 + \frac{2048}{3003}\tilde{y},$$

$$I_{16}(\tilde{y}) = \pi\tilde{y}^{15} + \frac{\pi}{2}\tilde{y}^{13} + \frac{3\pi}{8}\tilde{y}^{11} + \frac{5\pi}{16}\tilde{y}^9 + \frac{35\pi}{128}\tilde{y}^7 + \frac{63\pi}{256}\tilde{y}^5 + \frac{231\pi}{1024}\tilde{y}^3 + \frac{429\pi}{2048}\tilde{y}.$$

We note that $I_{2n}(\tilde{y})$ is a polynomial of degree \tilde{y}^{2n-1} , and $I_{2n+1}(\tilde{y})$ has a term involving $\ln|(1 + \sqrt{1-\tilde{y}^2})/\tilde{y}|$.

Appendix B. Expressions for submatrices in Eq. (32)

$$\begin{aligned} \mathbf{M}_{22}^s &= m_0^f \int_0^L \Psi_2(y) \Psi_2^T(y) dy, & \mathbf{M}_{aa}^s &= (2m_0^f + m_0^c) \int_0^L \Psi_a(y) \Psi_a^T(y) dy, \\ \mathbf{M}_{aw}^s &= m_2^c \int_0^L \Psi_a(y) \Psi_w^T(y) dy, & \mathbf{M}_{dd}^s &= (2m_0^f + m_0^c + m_2^c) \int_0^L \Psi_d(y) \Psi_d^T(y) dy, \\ \mathbf{M}_{dw}^s &= m_2^c \int_0^L \Psi_d(y) \Psi_w^T(y) dy, & \mathbf{M}_{wa}^s &= m_2^c \int_0^L \Psi_w(y) \Psi_a^T(y) dy, \\ \mathbf{M}_{ww}^s &= m_4^c \int_0^L \Psi_w(y) \Psi_w^T(y) dy, \end{aligned} \tag{B.1a-g}$$

where m_0^f , m_0^c , m_2^c and m_4^c are inertial coefficients defined as

$$\begin{aligned} m_0^f &\equiv \int_{-(t^c/2)-t^f}^{-t^c/2} \rho^f dx_3, & m_0^c &\equiv \int_{-t^c/2}^{t^c/2} \rho^c dx_3, \\ m_2^c &\equiv \int_{-t^c/2}^{t^c/2} \rho^c \left[\frac{4(x_3)^2}{(t^c)^2} - 1 \right] dx_3, & m_4^c &\equiv \int_{-t^c/2}^{t^c/2} \rho^c \left[\frac{4(x_3)^2}{(t^c)^2} - 1 \right]^2 dx_3. \end{aligned} \tag{B.2a-d}$$

$$\begin{aligned}
 \mathbf{K}_{22}^s &= (t^c A_{22}^c) \int_0^L \Psi_2'(y) \Psi_2'^T(y) dy + \alpha_{11} \int_0^L \Psi_2(y) \Psi_2^T(y) dy, \\
 \mathbf{K}_{2a}^s &= \alpha_{12} \int_0^L \Psi_2(y) \Psi_a^T(y) dy, \quad \mathbf{K}_{2w}^s = \alpha_{14} \int_0^L \Psi_2(y) \Psi_w^T(y) dy, \\
 \mathbf{K}_{a2}^s &= \alpha_{21} \int_0^L \Psi_a(y) \Psi_2^T(y) dy, \quad \mathbf{K}_{aw}^s = -\alpha_{24} \int_0^L \Psi_a'(y) \Psi_w^T(y) dy, \\
 \mathbf{K}_{aa}^s &= 2D_{22}^c \int_0^L \Psi_a''(y) \Psi_a'^T(y) dy + \alpha_{22} \int_0^L \Psi_a(y) \Psi_a'^T(y) dy, \\
 \mathbf{K}_{dd}^s &= 2D_{22}^c \int_0^L \Psi_d''(y) \Psi_d'^T(y) dy + \frac{4}{(t^c)^2} A_{33}^c \int_0^L \Psi_d(y) \Psi_d^T(y) dy, \\
 \mathbf{K}_{w2}^s &= \alpha_{41} \int_0^L \Psi_w(y) \Psi_2^T(y) dy, \quad \mathbf{K}_{wa}^s = \alpha_{42} \int_0^L \Psi_w(y) \Psi_a'^T(y) dy, \\
 \mathbf{K}_{ww}^s &= \frac{64D_{33}^c}{(t^c)^4} \int_0^L \Psi_w(y) \Psi_w^T(y) dy - \alpha_{44} \int_0^L \Psi_w'(y) \Psi_w'^T(y) dy.
 \end{aligned} \tag{B.3a-j}$$

The coefficients α_{ij} in expressions of \mathbf{K}_{2a}^s , \mathbf{K}_{2w}^s , etc. are defined as follows.

$$\begin{aligned}
 \alpha_{11} &= \frac{2}{t^c} A_{23}^c + \left(\frac{24D_{23}^c}{(t^c)^2} - 2A_{23}^c \right) \mathcal{R}_1, \\
 \alpha_{12} &= \left(1 + \frac{t^f}{t^c} \right) A_{23}^c + \left(\frac{24D_{23}^c}{(t^c)^2} - 2A_{23}^c \right) \mathcal{R}_2, \\
 \alpha_{14} &= \left[\frac{24D_{23}^c}{(t^c)^2} - 2A_{23}^c \right] \mathcal{R}_3 + \left[\frac{4D_{23}^c}{(t^c)^2} - A_{23}^c \right], \\
 \alpha_{21} &= -\left(1 + \frac{t^f}{t^c} \right) \alpha_{11}, \quad \alpha_{22} = -\left(1 + \frac{t^f}{t^c} \right) \alpha_{12}, \\
 \alpha_{24} &= -\left(1 + \frac{t^f}{t^c} \right) \alpha_{14}, \quad \alpha_{41} = \frac{2}{3} \alpha_{11}, \quad \alpha_{42} = \frac{2}{3} \alpha_{12}, \quad \alpha_{44} = \frac{2}{3} \alpha_{14}.
 \end{aligned}$$

where \mathcal{R}_1 , \mathcal{R}_2 and \mathcal{R}_3 are given in Eqs. (22a)–(22d).

The stiffness quantities are defined as

$$\begin{aligned}
 A_{23}^c &\equiv \int_{-t^c/2}^{t^c/2} G_{23}^c dx_3, \quad D_{23}^c \equiv \int_{-t^c/2}^{t^c/2} G_{23}^c(x_3)^2 dx_3, \quad A_{33}^c \equiv \int_{-t^c/2}^{t^c/2} Q_{33}^c dx_3, \\
 D_{33}^c &\equiv \int_{-t^c/2}^{t^c/2} Q_{33}^c(x_3)^2 dx_3, \quad D_{22}^f \equiv \int_{t^c/2}^{t^c/2+t^f} \bar{Q}_{22}^f \left(x_3 - \frac{t^c+t^f}{2} \right)^2 dx_3, \\
 F_{23}^c &\equiv \int_{-t^c/2}^{t^c/2} G_{23}^c(x_3)^4 dx_3, \quad A_{22}^f \equiv \int_{t^c/2}^{t^c/2+t^f} \bar{Q}_{22}^f dx_3,
 \end{aligned} \tag{B.6a-g}$$

where \bar{Q}_{22}^f is the reduced elastic constant.

In the approximation of the shape functions Ψ_a and Ψ_d in Eq. (25a,b) by polynomials, we denote transformation matrices as \mathbf{T}_a and \mathbf{T}_d , i.e.,

$$\Psi_a(y) \approx \mathbf{T}_a \mathbf{P}(y), \quad \Psi_d(y) \approx \mathbf{T}_d \mathbf{P}(y), \tag{B.7a, b}$$

in which $\mathbf{P}(y) = \{1, y, y^2, \dots, y^{N_p}\}^T$. Results computed in this paper are for $N_p = 16$, and $\mathbf{T}_a = \mathbf{T}_d$. By using the curve-fitting function *NonlinearRegress* in Mathematica® 6, \mathbf{T}_a is obtained as:

$$\mathbf{T}_a = \begin{bmatrix} 0.0 & 0.0 & 22.373 & -34.657 & 0.0 & 0.0 & 31.107 & -20.652 & 0.001763 & -0.00583 & 3.104 & -1.333 & 0.0389 & -0.0411 & 0.0956 & -0.0359 & 0.00449 \\ 0.0 & 0.0 & 61.673 & -161.567 & -0.023 & 0.35 & 648.886 & -716.972 & -56.699 & 161.363 & 152.084 & 176.373 & -596.009 & 471.691 & -162.855 & 21.7139 & 0.0 \\ 0.0 & 0.0 & 120.901 & -443.036 & -1.779 & 23.305 & 4706.35 & -6476.2 & -5434.6 & 17644.3 & -28454.4 & 62773.5 & -102332.0 & 97204.7 & -53031.4 & 15658.0 & -1957.25 \end{bmatrix} \tag{B.8}$$

We adopt the following three definitions:

$$II_k(y, t) \equiv a(t)^{k+1} \int_{-1}^{\tilde{y}} \sqrt{1 - \tilde{y}_0^2} I_k(\tilde{y}_0) d\tilde{y}_0 \Big|_{\tilde{y}=y/a(t)}, \quad t > 0, \tag{B.9a}$$

$$III_k^a(y, t) \equiv \sum_{j=1}^{N_p+1} \mathbf{T}_a(k, j) II_{j-1}(y, t), \quad III_k^d(y, t) \equiv \sum_{j=1}^{N_p+1} \mathbf{T}_d(k, j) II_{j-1}(y, t). \tag{B.9b, c}$$

Here, the operator $\mathbf{T}_a(k, j)$ denotes the (k, j) element of matrix \mathbf{T}_a . Same is for the operator $\mathbf{T}_d(k, j)$.

Submatrices associated with the unsteady hydrodynamic loads in Eq. (32) are defined as follows:

$$\begin{aligned} \mathbf{M}_{aa}^h &\equiv \frac{\rho_h}{\pi} \int_0^{a(t)} \Psi_a(y) \{III^a(y, t)\}^T dy, & \mathbf{C}_{aa}^h &\equiv \frac{2\rho_h}{\pi} \int_0^{a(t)} \Psi_a(y) \{\dot{III}^a(y, t)\}^T dy, \\ \mathbf{K}_{aa}^h &\equiv \frac{\rho_h}{\pi} \int_0^{a(t)} \Psi_a(y) \{\ddot{III}^a(y, t)\}^T dy, & \mathbf{M}_{ad}^h &\equiv -\frac{\rho_h}{\pi} \int_0^{a(t)} \Psi_a(y) \{III^d(y, t)\}^T dy, \\ \mathbf{C}_{ad}^h &\equiv -\frac{2\rho_h}{\pi} \int_0^{a(t)} \Psi_a(y) \{\dot{III}^d(y, t)\}^T dy, & \mathbf{K}_{ad}^h &\equiv -\frac{\rho_h}{\pi} \int_0^{a(t)} \Psi_a(y) \{\ddot{III}^d(y, t)\}^T dy, \\ \mathbf{E}_{aa}^h &\equiv \frac{\rho_h}{\pi} \int_0^{a(t)} \Psi_a(y) \{\ddot{II}(y, t)\}^T dy, \end{aligned} \quad (\text{B.10a-g})$$

$$\begin{aligned} \mathbf{M}_{da}^h &\equiv -\frac{\rho_h}{\pi} \int_0^{a(t)} \Psi_d(y) \{III^d(y, t)\}^T dy, & \mathbf{C}_{da}^h &\equiv -\frac{2\rho_h}{\pi} \int_0^{a(t)} \Psi_d(y) \{\dot{III}^a(y, t)\}^T dy, \\ \mathbf{K}_{da}^h &\equiv -\frac{\rho_h}{\pi} \int_0^{a(t)} \Psi_d(y) \{\ddot{III}^a(y, t)\}^T dy, & \mathbf{M}_{dd}^h &\equiv \frac{\rho_h}{\pi} \int_0^{a(t)} \Psi_d(y) \{III^d(y, t)\}^T dy, \\ \mathbf{C}_{dd}^h &\equiv \frac{2\rho_h}{\pi} \int_0^{a(t)} \Psi_d(y) \{\dot{III}^d(y, t)\}^T dy, & \mathbf{K}_{dd}^h &\equiv \frac{\rho_h}{\pi} \int_0^{a(t)} \Psi_d(y) \{\ddot{III}^d(y, t)\}^T dy, \\ \mathbf{E}_{dd}^h &\equiv -\frac{\rho_h}{\pi} \int_0^{a(t)} \Psi_d(y) \{\ddot{II}(y, t)\}^T dy, & \mathbf{c}_b &\equiv \{\tan \beta, 0, \dots, 0\}^T. \end{aligned} \quad (\text{B.10h-o})$$

Here, the vector $\{III\} \equiv \{III_1, III_2, \dots, III_{N_s}\}^T$, $\{\ddot{II}\} \equiv \{\ddot{II}_1, \ddot{II}_2, \dots, \ddot{II}_{N_p}\}^T$, a superimposed dot denotes differentiation with respect to time t , and \mathbf{c}_b is $N_p \times 1$ vector.

Appendix C. Discrete-time representation of Eq. (33)

In the sampling period $t \in [t_k, t_{k+1})$, it is assumed that the system matrix $\mathcal{A}(t)$ and the generalized hydrodynamic load vector $\mathbf{Q}(t)$ in Eq. (33) remain unchanged; $\mathcal{A}(t) = \mathcal{A}[t_k]$, $\mathbf{Q}(t) = \mathbf{Q}[t_k]$. Using the forward-difference method, the solution of Eq. (33) can be written as

$$\mathbf{x}(t) = e^{\mathcal{A}[t_k](t-t_k)} \mathbf{x}[t_k] + \int_{t_k}^t e^{\mathcal{A}[t_k](t-\tau)} d\tau \mathbf{Q}[t_k]. \quad (\text{C.1})$$

At time $t = t_{k+1}$, Eq. (C.1) becomes

$$\mathbf{x}[t_{k+1}] = e^{\mathcal{A}[t_k]\Delta t} \mathbf{x}[t_k] + \int_0^{\Delta t} e^{\mathcal{A}[t_k]\tau} d\tau \mathbf{Q}[t_k]. \quad (\text{C.2})$$

Recurrence relation (C.2) is the desired discrete-time representation of the state-space Eq. (33). The group property (Meirovitch, 1997) can be used to efficiently evaluate the transition matrix $e^{\mathcal{A}[t_k]\Delta t}$ and the integral in Eq. (C.2) by dividing Δt into smaller intervals.

References

- ABAQUS, 2004. ABAQUS[®] analysis user's manual, version 6.5.
- Barut, A., Madenci, E., Heinrich, J., Tessler, A., 2001. Analysis of thick sandwich construction by a {3,2}-order theory. *International Journal of Solids and Structures* 38, 6063–6077.
- Batra, R.C., Vidoli, S., 2002. Higher-order piezoelectric plate theory derived from a three-dimensional variational principle. *AIAA Journal* 40 (1), 91–104.
- Batra, R.C., Vidoli, S., Vestroni, F., 2002. Plane wave solutions and modal analysis in higher order shear and normal deformable plate theories. *Journal of Sound and Vibration* 257 (1), 63–88.
- Bereznitski, A., 2001. Slamming: the role of hydroelasticity. *International Shipbuilding Progress* 48 (4), 333–351.
- Bishop, R., Price, W.G., Tam, P.K.Y., 1978. On the dynamics of slamming. *Transactions of the Royal Institution of Naval Architects* 120, 259–280.
- Chu, W.H., Abramson, H.N., 1961. Hydrodynamic theories of ship slamming-review and extension. *Journal of Ship Research* 4 (4), 9–21.
- Erdélyi, A., Magnus, W., Oberhettinger, F., Tricomi, F., 1954. *Tables of Integral Transforms*. Bateman Manuscript Project, vol. 2. McGraw-Hill Book Company, Inc..
- Faltinsen, O.M., 1990. *Sea Loads on Ships and Offshore Structures*. Cambridge Ocean Technology Series. Cambridge University Press, Cambridge, Great Britain, pp. 282–296.
- Faltinsen, O.M., 1997. The effect of hydroelasticity on ship slamming. *Philosophical Transactions of the Royal Society of London A* 355, 575–591.
- Faltinsen, O.M., 1999. Water entry of a wedge by hydroelastic orthotropic plate theory. *Journal of Ship Research* 43 (3), 180–193.
- Faltinsen, O.M., 2000. Hydroelastic slamming. *Journal of Marine Science and Technology* 5, 49–65.
- Faltinsen, O.M., 2002. Water entry of a wedge with finite deadrise angle. *Journal of Ship Research* 46 (1), 39–51.
- Faltinsen, O.M., Chezhan, M., 2005. A generalized wagner method for three-dimensional slamming. *Journal of Ship Research* 49 (4), 279–287.
- Faltinsen, O.M., Landrin, M., Greco, M., 2004. Slamming in marine applications. *Journal of Engineering Mathematics* 48, 187–217.
- Gakhov, F.D., 1966. *Boundary Value Problems* (I.N. Sneddon, Trans.). Addison-Wesley, pp. 426–428.
- Hayman, B., 1993. Response of sandwich structures to slamming and impact loads. In: Shenoi, R.A., Wellicome, J.F. (Eds.), *Composite Materials in Marine Structures*, vol. 2. Cambridge University Press, Cambridge, Great Britain (Chapter 9).
- Hohe, J., Librescu, L., 2003. A nonlinear theory for doubly curved anisotropic sandwich shells with transversely compressible core. *International Journal of Solids and Structures* 40, 1059–1088.
- Howison, S.D., Ockendon, J.R., Wilson, S.K., 1991. Incompressible water-entry problems at small deadrise angles. *Journal of Fluid Mechanics* 222, 215–230.

- Katz, J., Plotkin, A., 1991. *Low-Speed Aerodynamics: From Wing Theory to Panels Methods*. McGraw-Hill, New York. pp. 69–71.
- Khabakhpasheva, T.I., 2005. Impact of a surface wave on an elastic hull. *Fluid Dynamics* 41 (3), 424–433. translated from *Izvestiya Rossiiskoi Akademii Nauk, Mekhanika Zhidkosti i Gaza*, No. 3, 2006. pp. 114–124.
- Korobkin, A., 1995. Wave impact on the bow end of a catamaran wet deck. *Journal of Ship Research* 39 (4), 321–327.
- Korobkin, A.A., 2007. Second-order wagner theory of wave impact. *Journal of Engineering Mathematics* 58, 121–139. doi:10.1007/s10665-006-9105-7.
- Korobkin, A.A., Scolan, Y.-M., 2006. Three-dimensional theory of water impact. Part 2. Linearized wagner problem. *Journal of Fluid Mechanics* 549, 343–373.
- Kvålsvold, J., Faltinsen, O., 1995. Hydroelastic modeling of wet deck slamming on multihull vessels. *Journal of Ship Research* 39 (3), 225–239.
- Librescu, L., Meirovitch, L., Na, S.S., 1997. Control of cantilever vibrations via structural tailoring and adaptive materials. *AIAA Journal* 35 (8), 1309–1315.
- Mei, X., Liu, Y., Yue, D.K.P., 1999. On the water impact of general two-dimensional sections. *Applied Ocean Research* 21, 1–15.
- Meirovitch, L., 1997. *Principles and Techniques of Vibrations*. Prentice Hall, Upper Saddle River, New Jersey.
- Mizoguchi, S., Tanizawa, K., 1996. Impact wave loads due to slamming – a review. *Ship Technology Research* 43, 139–154.
- Oliver, J.M., 2007. Second-order wagner theory for two-dimensional water-entry problems at small deadrise angles. *Journal of Fluid Mechanics* 572, 59–85.
- Palazotto, A.N., Linnemann, P.E., 1991. Vibration and buckling characteristics of composite cylindrical panels incorporating the effects of a higher order shear theory. *International Journal of Solids and Structures* 28 (3), 341–361.
- Peseux, B., Gornet, L., Donguy, B., 2005. Hydrodynamic impact: numerical and experimental investigations. *Journal of Fluids and Structures* 21, 277–303.
- Scolan, Y.M., 2004. Hydroelastic behavior of a conical shell impacting on a quiescent-free surface of an incompressible liquid. *Journal of Sound and Vibration* 277, 163–203.
- Scolan, Y.M., Korobkin, A.A., 2001. Three-dimensional theory of water impact. Part I: inverse Wagner problem. *Journal of Fluid Mechanics* 440, 293–326.
- Stavovy, A.B., Chuang, S.-L., 1976. Analytical determination of slamming pressures for high-speed vehicles in waves. *Journal of Ship Research* 20 (4), 190–198.
- Takagi, K., 2004. Numerical evaluation of three-dimensional water impact by the displacement potential formulation. *Journal of Engineering Mathematics* 48, 339–352.
- Toyama, Y., 1993. Two-dimensional water impact of unsymmetrical bodies. *Journal of the Society of Naval Architects of Japan* 173, 285–291 (in Japanese).
- Vorus, W.S., 2000. Shock reduction in planing boats. United States Patent, No. 6158376.
- Vorus, W.S., 2004. A compliant-hull concept for planing craft wave-impact shock reduction. *Journal of Engineering Mathematics* 48, 253–277.
- Wagner, V.H., 1932. Phenomena associated with impact and sliding on liquid surfaces. *NACA Transaction* 1366, translated from *ZAMM*, vol. 12, pp.193–215.
- Wolfram Research, Inc., 2007. *Mathematica*®6.
- Wu, G.X., Sun, H., He, Y.S., 2004. Numerical simulation and experimental study of water entry of a wedge in free fall motion. *Journal of Fluids and Structures* 19, 277–289.
- Yettou, E.-M., Desrochers, A., Champoux, Y., 2007. A new analytical model for pressure estimation of symmetrical water impact of a rigid wedge at variable velocities. *Journal of Fluids and Structures* 23, 501–522.
- Zhao, R., Faltinsen, O., 1993. Water entry of two-dimensional bodies. *Journal of Fluid Mechanics* 246, 593–612.